NOAA Technical Report EDS 13

Precipitation Analysis for BOMEX Period III

September 1975

DEPARTMENT OF COMMERCE ★ UNITED STATES OF AMERICA ★

noaa NATIONAL OCEANIC AND ATMOSPHERIC ADMINISTRATION / Environmental Data Service

AMERICAN REVOLUTION BICENTENNIAL 1776-1976

NOAA TECHNICAL REPORTS

Environmental Data Service Series

The Environmental Data Service (EDS) archives and disseminates a broad spectrum of environmental data gathered by the various components of NOAA and by the various cooperating agencies and activities throughout the world. The EDS is a "bank" of worldwide environmental data upon which the researcher may draw to study and analyze environmental phenomena and their impact upon commerce, agriculture, industry, aviation, and other activities of man. The EDS also conducts studies to put environmental phenomena and relations into proper historical and statistical perspective and to provide a basis for assessing changes in the natural environment brought about by man's activities.

The EDS series of NOAA Technical Reports is a continuation of the former series, the Environmental Science Services Administration (ESSA) Technical Report, EDS.

Reports in the series are available from the National Technical Information Service, U.S. Department of Commerce, Sills Bldg., 5285 Port Royal Road, Springfield, Va. 22151. Price: $3.00 paper copy; $1.45 microfiche. When available, order by accession number shown in parentheses.

ESSA Technical Reports

EDS 1 Upper Wind Statistics of the Northern Western Hemisphere. Harold L. Crutcher and Don K. Halligan, April 1967. (PB-174-921)

EDS 2 Direct and Inverse Tables of the Gamma Distribution. H. C. S. Thom, April 1968. (PB-178-320)

EDS 3 Standard Deviation of Monthly Average Temperature. H. C. S. Thom, April 1968. (PB-178-309)

EDS 4 Prediction of Movement and Intensity of Tropical Storms Over the Indian Seas During the October to December Season. P. Jagannathan and H. L. Crutcher, May 1968. (PB-178-497)

EDS 5 An Application of the Gamma Distribution Function to Indian Rainfall. D. A. Mooley and H. L. Crutcher, August 1968. (PB-180-056)

EDS 6 Quantiles of Monthly Precipitation for Selected Stations in the Contiguous United States. H. C. S. Thom and Ida B. Vestal, August 1968. (PB-180-057)

EDS 7 A Comparison of Radiosonde Temperatures at the 100-, 80-, 50-, and 30-mb Levels. Harold L. Crutcher and Frank T. Quinlan, August 1968. (PB-180-058)

EDS 8 Characteristics and Probabilities of Precipitation in China. Augustine Y. M. Yao, September 1969. (PB-188-420)

EDS 9 Markov Chain Models for Probabilities of Hot and Cool Days Sequences and Hot Spells in Nevada. Clarence M. Sakamoto, March 1970. (PB-193-221)

NOAA Technical Reports

EDS 10 BOMEX Temporary Archive Description of Available Data. Terry de la Moriniere, January 1972. (COM-72-50289)

EDS 11 A Note on a Gamma Distribution Computer Program and Graph Paper. Harold L. Crutcher, Gerald L. Barger, and Grady F. McKay, April 1973. (COM-73-11401)

EDS 12 BOMEX Permanent Archive: Description of Data. Center for Experiment Design and Data Analysis, May 1975.

NOAA Technical Report EDS 13

Precipitation Analysis for BOMEX Period III

Center for Experiment Design and Data Analysis

M.D. Hudlow and W.D. Scherer

September 1975

UNITED STATES DEPARTMENT OF COMMERCE
Rogers C. B. Morton, Secretary

NATIONAL OCEANIC AND ATMOSPHERIC ADMINISTRATION
Robert M. White, Administrator

National Weather Service
George P. Cressman, Director

CONTENTS

ABSTRACT

Radar, satellite, and rain-gage data are used qualitatively and quantitatively to describe the precipitation morphology for 10 days (June 21 to 30, 1969) of Period III of the Barbados Oceanographic and Meteorological Experiment (BOMEX). Typical satellite and radar photographs are presented to illustrate cloud patterns and precipitation echoes for both "undisturbed" and "disturbed" weather. Undisturbed conditions are shown to prevail for 5 consecutive days and moderately disturbed conditions for 2 days.

Procedures for calibrating and optimizing the use of the quantitative radar data are discussed. Satellite cloud data are used to extrapolate the rainfall estimates to areas not covered by radar. The quantitative rainfall computations gave average rainfall rates over the BOMEX square (250,000 km^2) of 0.35 mm/day and 3.7 mm/day for the 5-day undisturbed and 2-day disturbed periods, respectively. Based on the results from an error analysis and on independent comparisons against atmospheric water budget analyses, it is concluded that the magnitudes of the errors accompanying the precipitation estimates for both periods probably are small compared with either the total precipitation or evaporation.

The spatial distributions of intensity in the BOMEX echoes are highly nonlinear, and the total echo area is shown to depend on the technical characteristics of the radar hardware. These findings stress the importance of careful experimental design for the radar and satellite programs of future tropical oceanic experiments.

PRECIPITATION ANALYSIS FOR BOMEX PERIOD III

M.D. Hudlow and W.D. Scherer
Center for Experiment Design and Data Analysis
Environmental Data Service
National Oceanic and Atmospheric Administration
Washington, D.C. 20235

1. INTRODUCTION

The "Core Experiment" of the Barbados Oceanographic and Meteorological Experiment (BOMEX) was designed for study of sea-air interactions through determination of the heat, momentum, and water budgets. During the field operations conducted in the summer of 1969, atmospheric sampling was concentrated within a 500-km x 500-km x 500-mb "box" east of the island of Barbados. Ocean salinity and temperature were measured routinely to a depth of 1,000 m.

For budget studies, a knowledge of the type and quantity of clouds and precipitation within the experimental volume is needed. Surface-based and airborne radars, shipboard rain gages, and infrared and visible sensors carried on satellites provided data for evaluating the precipitation term in the budget equations. These equations have been formulated by Rasmusson (1971).

To meet the objectives of the Core Experiment, primary emphasis was placed on the first three BOMEX Observations Periods (May 3 to 15, May 24 to June 10, and June 19 to July 2, 1969). The precipitation analysis for Period III presented here extends from June 21 to June 30, 1969. The precipitation morphology is described, and time and space distributions of cloud and echo cover and precipitation estimates for periods as short as 6 hr are presented.

Various other aspects of the Core Experiment and results of continuing analyses of BOMEX data have been discussed by Holland (1970, 1972a and b) and Holland and Rasmusson (1973). For an overall description of BOMEX, including sensors used and experiments carried out by individual investigators, the reader is referred to BOMEX Field Observations and Basic Data Inventory (BOMAP Office, 1971).

2. MEANS OF DATA COLLECTION

Land-based, shipboard, and airborne radar observations were used to document precipitation echoes. Location of the two surface radars and the flight track for the aircraft radar photography are shown in figure 1. Both visible and infrared satellite data augmented the radar coverage. Sources of other supplementary data were rain gages mounted on each of the five BOMEX fixed ships--four stationed at the corners of the BOMEX square and one in the center--and a rain-gage network on Barbados.

2.1 Surface Radars and Digitization of Radar Data

The primary quantitative data for the southern half of the BOMEX box were obtained with a U.S. Army MPS-34 radar stationed on the island of Barbados and a METEOR-200 radar aboard the NOAA ship Discoverer, located at the southeastern corner of the BOMEX square. Characteristics of these two X-band radars are listed in table 1.

The METEOR-200 basic equipment is similar to the MPS-34 radar, which has been described by Hudlow (1970a). The antenna and pedestal unit were mounted on a gyro-stabilized platform that compensated for the ship's roll up to ± 25° and pitch up to ± 10°. "Gain-stepping" of the radar receiver and scope photography were used in recording storm intensities with both radar sets.

To permit quantitative analyses by computer, the photographic data obtained by the island and Discoverer radars during BOMEX Periods II and III were digitized with a coordinate digitizer. Additional information on the procedures used and a detailed inventory of these data are given in NOAA Technical Report EDS 12 (Center for Experiment Design and Data Analysis, 1975).

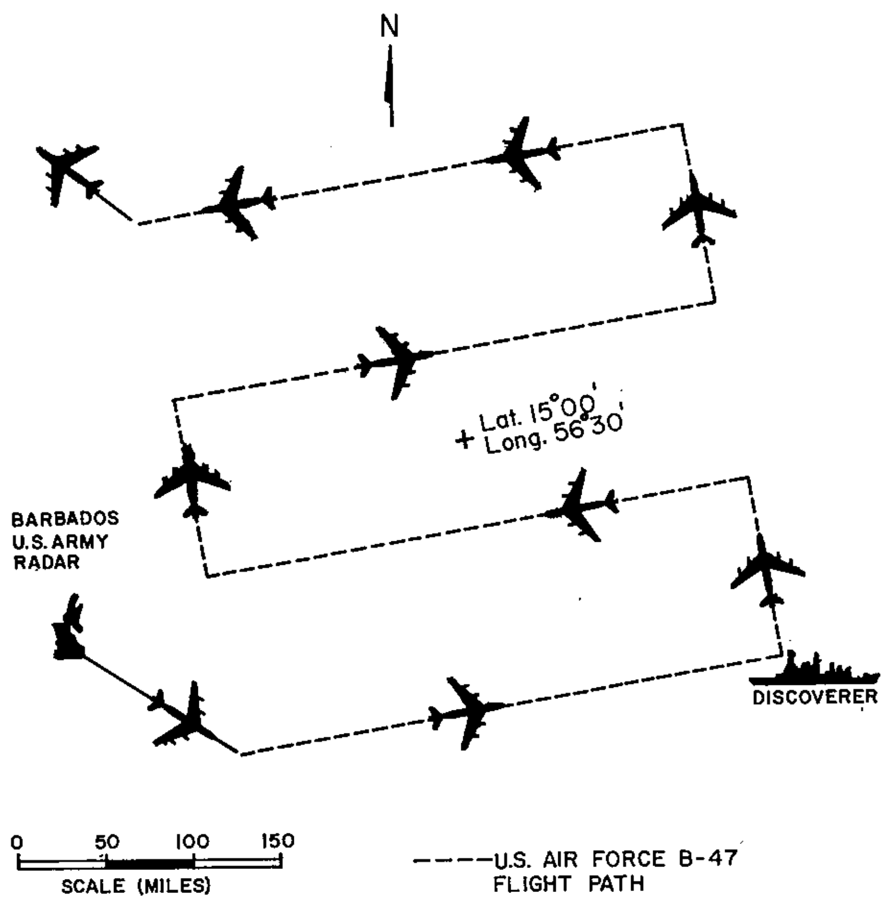

Figure 1.--Positions of surface-based radars and radar aircraft flight track used during BOMEX.

Table 1.--Characteristics of the MPS-34 and METEOR-200 radars (long pulse)

Characteristics	Nominal value	
	MPS-34	METEOR-200
Transmitted power (peak)	180 kW	175 kW
Wavelength	3.2 cm	3.2 cm
Antenna shape	Parabolic	Parabolic
Horizontal and vertical beam widths	1°	1.25°
Minimum detectable signal	-105 dBm	-97 dBm
Pulse repetition frequency	180 pps	240 pps
Pulse width	5×10^{-6} s	3×10^{-6} s

2.2 Airborne Radars

A U.S. Air Force WB-47 aircraft equipped with an APS-64 radar collected radar photographs once daily along the flight path shown in figure 1 at an altitude of about 9 km. The APS-64 is an X-band system with 3.5° horizontal and 5° vertical beam widths. Mosaics of radar photographs obtained with this radar have been prepared for several days during BOMEX Period III as a qualitative means for identifying precipitation areas. Examples of this type of presentation are given in BOMEX Period III Radar-Satellite Atlas (Scherer and Hudlow, 1975). As an additional aid, radar films obtained by NOAA's Research Flight Facility aircraft were scanned on microfilm.

2.3 Satellite Measurements

Infrared data from the Nimbus-3 satellite and visible data from the Applications Technology Satellite 3 (ATS-3) provided supplementary coverage of the area included in the precipitation analysis. Nimbus-3 high resolution infrared (HRIR) data were obtained once a day at approximately local midnight. Three gridded and enlarged ATS-3 photographs were available for each day--shortly after sunup, around midday, and close to sundown. Located above a subsatellite point near the BOMEX area, ATS-3 provided a spatial resolution of about 4 km at the subsatellite point.

The ground resolution at a subsatellite point for the Nimbus-3 HRIR radiometer scanning system is approximately 8.5 km (Sabatini, Ed., Nimbus III User's Guide). The gridding accuracy of both the visible and infrared products used in this study is believed to lie within about 45 km.

2.4 Rain-Gage Measurements

A rain-gage was mounted on a boom extending from the bow of each of the five BOMEX fixed ships. Consisting of a collector 7.5 cm in diameter and an attached hose for depositing the collected precipitation into a clear cylinder graduated to the nearest quarter of a millimeter, the gage was mounted, non-gimbaled, at deck level about 6 m from the tip of the bow. Cumulative precipitation amounts to the nearest 1 mm were manually recorded and transcribed onto surface observation forms every 1.5 hr.

Rainfall estimates were also obtained from a rain-gage network in the extreme southeast part of Barbados. Use of these data, as well as those obtained with the shipboard gages, is discussed in section 4.

3. WEATHER SYSTEMS AS REVEALED BY RADAR AND SATELLITE PHOTOGRAPHS

A complete sequence of radar and visible and infrared satellite pictures for synoptic times from June 21 through July 2, 1969, is given in the BOMEX Period III Radar-Satellite Atlas cited earlier. Typical photographs are presented here to illustrate general weather conditions during the period of interest. Visible satellite photographs for all four BOMEX Observation Periods (May 3 through July 28, 1969) are contained in BOMEX Atlas of Satellite Cloud Photographs (Myers, 1971).

The 5 days from June 22 through June 26 were largely free of convective disturbances. Figures 2 and 3 typify the radar echo and satellite cloud patterns during these 5 days. Of importance is that most of the cloud cover in the satellite photograph over the BOMEX square (fig. 3) is not accompanied by precipitation echoes as revealed by the radar photographs (fig. 2), and that this cloud cover lies predominantly over the southern half of the BOMEX square.

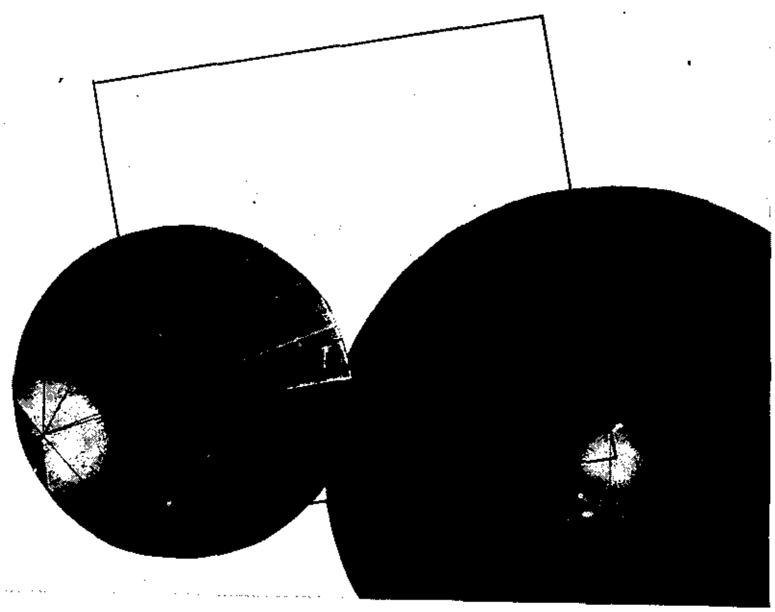

Figure 2.--Composite of surface-based radar photographs for June 23, 1969, 1630 local time (l.t.), with BOMEX square illustrated.

The 5-day undisturbed period was bracketed by two convective disturbances, a moderate one that moved out of the BOMEX box late on June 21 and a mild one that moved in late on June 26 and early June 27. This 5-day interval between disturbances is slightly greater than the mean interval of approximately 3.5 days obtained from data presented by Frank (1970), who identified and categorized the Atlantic tropical systems for 1969 according to a scheme that places primary emphasis on synoptic-scale perturbations in the wind and pressure fields. Since conventional radiosonde data and surface observations are scarce for ocean areas, satellite photographs are of particular importance in identifying such perturbations.

On June 28 an organized convective system entered the BOMEX box from the east. This disturbance persisted through the morning hours of June 29, and at the time of the radar composite photograph, 0722 local time (l.t.), shown in figure 4, significant wave features are revealed by both the radar echo and the satellite cloud patterns (fig. 5).

Frank (1970) considers two broad categories of disturbances, depending on the main source of energy: (1) those drawing primarily on latent heat, and (2) those feeding mainly on a baroclinic source of energy. For example, the first category includes intertropical convergence zone (ITCZ) disturbances and tropical waves, while the second includes upper cold lows. Following Frank's classification, the disturbances passing the Barbados area on June 21, June 27, and June 29 were all tropical waves originating over the African continent. The waves on June 21 and June 29 produced wind shifts at San Andres, but the wave that passed Barbados on June 27 weakened and dissipated in the Caribbean (Frank, 1970).

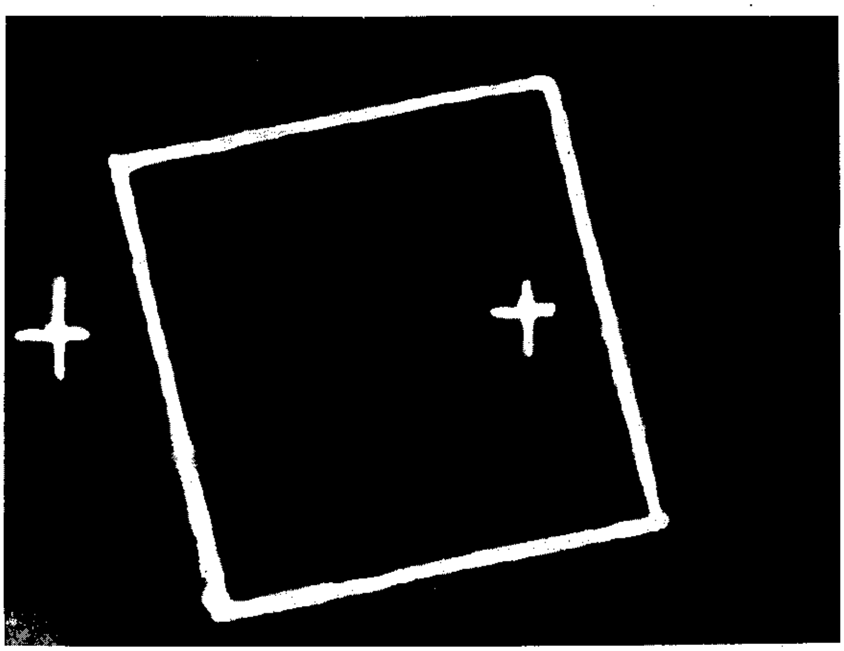

Figure 3.--Enlargement of ATS-3 satellite photograph for June 23, 1969, 1630 l.t., with BOMEX square illustrated.

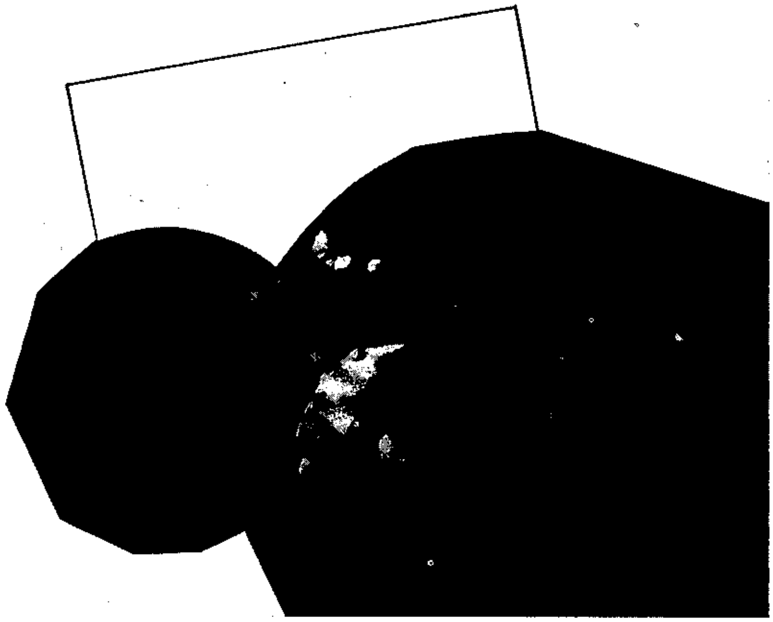

Figure 4.--Composite of surface-based radar photographs for June 29, 1969, 0722 l.t., with BOMEX square illustrated.

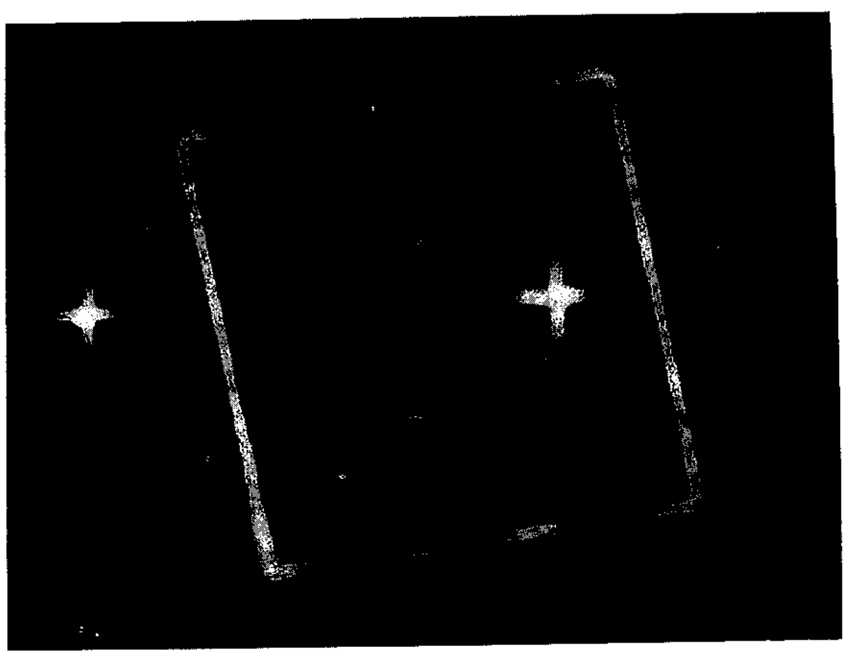

Figure 5.--Enlargement of ATS-3 satellite photograph for June 29, 1969, 0719 l.t., with BOMEX square illustrated.

4. ANALYTICAL PROCEDURES

The quantitative data collected with the two surface-based radars form the primary building blocks for deriving rainfall estimates. Since only a small portion of the BOMEX square (12 percent) was covered by radar measurements at ranges suitable for quantitative gain-step estimates, an alternative statistical approach was sought for deriving rainfall estimates. A statistical model of radar echoes was developed (see appendix) to estimate echo area, height, and rainfall using echo length as the independent variable.

4.1 Analysis of Shipboard Rain-Gage Data

The rain-gage data were used in their raw tabulated form, except in instances where obvious observer errors were spotted by cross-checking against the event and radar "bench" logbooks. Arithmetic averages for the BOMEX box were computed from the rain-gage measurements made aboard the five ships. Because of the low gage density represented by this network and since the accuracy of shipboard rain-gage measurements generally are inferior to measurements on land, the results discussed in section 5.3 serve only as a relative consistency check. The radar and satellite data remain the principal sources for deriving quantitative precipitation estimates.

4.2 Calibrations of Surface-Based Radars and Analysis of Radar Data

The approach adopted here for deriving rainfall estimates from radar intensity measurements is the conventional one of solving the radar equation and an equation relating the rainfall rate to the equivalent reflectivity factor.

The following steps were taken for hardware calibration and overall calibration and analysis:

(1) Conventional hardware and film calibrations were performed daily in the field.

(2) A drop-size distribution, based on drop-size data collected at a location with a climatology similar to that of Barbados, was adopted.

(3) Rainfall estimates derived from measurements made with the island radar were compared with those obtained from a rain-gage network covering a 90-km^2 area on Barbados.

(4) For a 1-hr test on June 18, 1969, between BOMEX Periods II and III, while the Discoverer was berthed in Barbados, data collected with the island radar were compared with measurements made with the shipboard radar for areas of overlapping coverage.

(5) Corrections for attenuation due to oxygen, water vapor, and rainfall were derived.

(6) An empirical time-averaged adjustment factor for non-beam filling for ranges beyond 160 km was calculated.

The field calibrations for the island radar are documented in an earlier publication by Hudlow (1970a). Analogous field calibrations were performed for the shipboard system.

4.2.1 Radar Equation and Drop-Size Distribution

The average power, $\overline{P}_r$, received at the radar antenna from a volume of precipitation particles filling a nonattenuated radar beam is given by Probert-Jones (1962):

$$\overline{P}_r = \left[\left(\frac{\pi^3}{710}\right)\left(\frac{P_t G^2 h \theta^2}{\lambda^2}\right)\right]\left[|K|^2 \frac{Z_e}{r^2}\right] , \quad (1)$$

where P_t is the transmitted power, G is the antenna gain, h is the pulse width (distance units), θ is the beam width, λ is the wavelength, and

$$K = (m^2 - 1)/(m^2 + 2) \quad ,$$

where m is the complex index of refraction of the precipitation particles, Z_e is the target equivalent reflectivity factor, and r is the slant range to the target. Standard gain-horn measurements were not made during BOMEX. Antenna gain was computed from the expression given by Probert-Jones (1962),

$$G = \pi^2/\theta^2 \quad . \quad (2)$$

The term in the first bracket on the right side of eq. (1)--called the radar constant--depends only on the radar hardware. Solving for Z_e from eq. (1) gives

$$Z_e = (r^2\overline{P}_r)/(C\ |K|^2) \quad ; \quad (3)$$

where C is the radar constant. Since $\overline{P}_r$ and r are explicitly given by radar measurements and C and $|K|^2$ are assumed constant for a particular radar, Z_e can be evaluated from eq. (3).

The magnitude of Z_e is related to the number and size of hydrometeors in the pulse volume. Also, the rainfall rate, R, is related to the drop-size distribution, which depends upon location, rain type, season, and other factors.

Empirical relationships relating rainfall rate to reflectivity have been derived from drop-size spectra collected at the earth's surface for several geographic locations (e.g., Mueller and Sims, 1969). Majuro in the Marshall Islands is climatologically similar to the Barbados vicinity. The Marshall Islands relationship given by Mueller and Sims was therefore applied to the BOMEX radar data:

$$R = 0.018 Z_e^{0.745} \quad , \quad (4)$$

where R is the rainfall rate in mm/hr, and Z_e is the equivalent reflectivity factor in mm^6/m^3.

4.2.2 Overall Calibration Derived From Comparison of Island Radar and Island Rain-Gage Data

Rainfall estimates derived from the MPS-34 radar for 5 hr of data from four storms--one for each BOMEX Observation Period--were compared with those obtained from a rain-gage network inside a 90-km^2 area in the extreme southeast part of the island (fig. 6). Attenuation from rainfall between the radar site and the rain-gage network was subjectively estimated to be small during the periods chosen for comparison. Criteria used for storm selection required that the storms originate over oceanic areas to the southeast of Barbados and move in a northwesterly direction over the gage network. Because of ground clutter interference, it was impossible to evaluate the rainfall attenuation correction described in section 4.2.4; therefore, only periods with small intervening rainfall between the radar and gage network were selected for comparison.

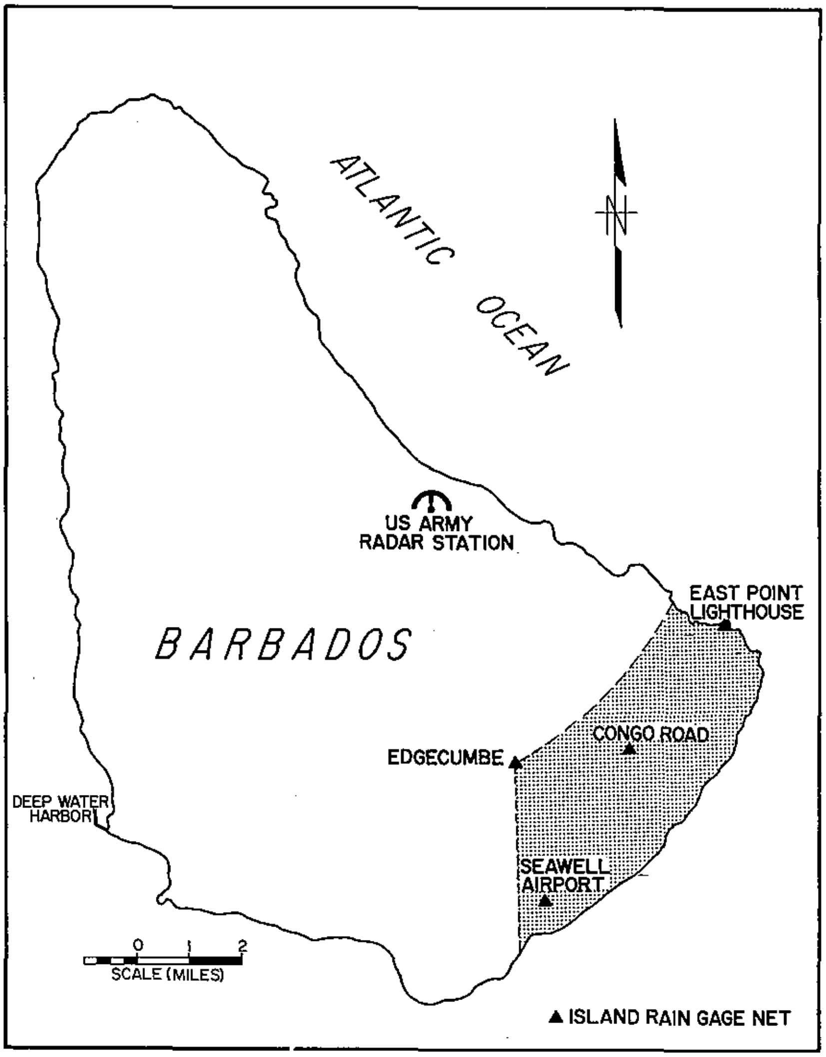

Figure 6.--Radar site and rain-gage network on the island of Barbados.

Table 2, which summarizes the results of the radar-gage comparisons, shows the estimates based on the radar data to be lower than those from the rain-gage analysis. Certain inaccuracies entering the solution of the radar equation will normally lead to underestimates, as have been reported by many investigators (e.g., Jones and Bigler, 1966), but the exact reason for the MPS-34 radar underestimates is not known. One likely source of error is that eq. (2) gives an overestimate for antenna gain (sec. 4.2.1).

Since the gage-to-radar ratios are consistent to better than a factor of 2 for all storms, the radar gain-setting calibrations reported by Hudlow (1970a) were adjusted for a mean bias of 9 dB in received power. This corresponds to a factor of 4.7 (the mean of the gage-to-radar ratios) in the rain-rate estimates when eq. (4) is used. The threshold values for the gain settings of the shipboard radar were adjusted by the same magnitude since a comparison of data from the two radars for the same echoes did not reveal any significant differences in intensity measurements.

Other alternatives could have been used for deriving the mean calibration factor from the data given in table 2. The rms error would be smaller if a correction factor given by $\Sigma G_i/\Sigma R_i$ were applied instead of $[\Sigma(G_i/R_i)]/5$. However, the latter has the advantages of giving radar estimates that are (1) all within a factor of 2 of the gage estimates, and (2) are close to those obtained from the linear least-squares model, $\hat{G}_i = \beta_o + \beta_1 R_i$, where the estimator for G_i is taken as the adjusted radar estimates.

Table 2.--Hourly radar rainfall estimates, averaged over the area of the Barbados rain-gage network, compared with those derived from the rain-gage measurements and with the radar estimates adjusted by the mean gage-to-radar ratio

Date and time (l.t.)	MPS-34 radar (mm)	Rain-gage network (mm)	Gage-to-radar ratio	Radar times mean gage-to-radar ratio (mm)
May 13, 1969 0300-0400	0.36	2.44	6.78	1.69
May 31, 1969 0400-0500	0.38	1.27	3.34	1.79
June 20, 1969 1500-1600	0.53	2.29	4.32	2.49
June 20, 1969 1600-1700	3.32	10.11	3.05	15.60
July 18, 1969 1300-1400	0.25	1.50	6.00	1.18
		Total	23.49	

$$[\Sigma(G_i/R_i)]/5 = \overline{G/R} = 4.7$$

4.2.3 Comparison Between MPS-34 and METEOR-200 Radars

On June 18, 1969, between BOMEX Periods II and III, while the *Discoverer* was berthed in Deep Water Harbor, Barbados, continuous gain-step measurements were made for 1 hr with the MPS-34 and the METEOR-200 radars. Twelve echoes observed within 160 km of the radar sites were sampled during this period.

After normalization for differences in radar constants, target ranges, and system sensitivities, the intensity measurements made with the two radars were compared. The results showed no discrepancies greater than 2 dB, which is within the accuracy of the calibration equipment and procedures, and it was concluded that the measurements made by the two radars were in agreement.

4.2.4 Attenuation Corrections

X-band transmissions are susceptible to attenuation by precipitation and atmospheric gases between the radar site and the target. Rainfall attenuation is of greatest concern, since (1) the source is highly transient, and (2) such attenuation can become quite large. Also, for long path lengths in a tropical atmosphere, attenuation by oxygen and water vapor becomes significant.

Attenuation corrections for atmospheric gases can be made relatively easily, as they depend only on atmospheric pressure and relative humidity, and approximate data for these two parameters are generally available. Table 3 contains attenuation values for a mean tropical atmosphere, valid for use in correcting the BOMEX radar data.

Amending eq. (3) to include an adjustment for attenuation resulting from rainfall yields

$$Z_e = (r^2 \overline{P}_r \, e^{2\int_o^r \gamma dr})/(C \, |K|^2) \quad , \tag{5}$$

where the exponential term accounts for liquid-water attenuation, γ is the attenuation coefficient (dB per unit distance), and r is the slant range.

Table 3.--Attenuation by oxygen and water vapor for X-band radiation emitted at 0° tilt angle and passing through a mean tropical atmosphere along various path lengths

One-way path to target (km)	Total two-way attenuation by H_2O and O_2 (dB)
48	1.4
64	1.9
80	2.3
96	2.8
112	3.2
128	3.6
144	4.0
160	4.3

Theoretically, given the distribution of the attenuation coefficient, γ, along the path, eq. (5) can be used to solve for Z_e. Since γ is a function of the drop-size distribution, and since drop sizes vary with time and location, a unique γ distribution along the path cannot be determined. It is possible, however, to empirically relate γ to Z_e or R. One such relationship, based on the drop-size distribution adopted for this study (sec. 4.2.1), is

$$\gamma = 0.012R \quad , \tag{6}$$

where γ is in dB/km and R is in mm/hr. Conceptually, one approach could consist of using eqs. (4), (5), and (6) to derive rainfall estimates, adjusted for attenuation by liquid water, by starting the solution at the radar site and proceeding outward; but, as pointed out by Hitschfeld and Bordan (1954), this can result in larger errors than will occur if no attempt is made to correct for attenuation. The coefficients in eq. (4), and to a somewhat lesser degree, the one in eq. (6), are sensitive to change in the drop-size distribution. Relatively small errors in these coefficients can result in significant errors in the estimates of R, especially at remote ranges, since the error accumulates with increasing range from the radar site as the integration of eq. (5) is performed.

In view of the above, the following procedure was adopted for processing BOMEX gain-step data:

(1) All initial estimates for R were derived by use of eqs. (3) and (4), uncorrected for attenuation by liquid water.

(2) Attenuation adjustments were made to yield final R estimates, by first using eqs. (5) and (6), with the array of R's held fixed and equal to the first estimates, and then by solving for a final set of R's from eq. (4).

Although this procedure may not compensate sufficiently for the true effects of rainfall attenuation, it should not result in unrealistically large corrections, which can result if the R's are adjusted as the integration in eq. (5) is performed and the estimate for each successively greater range is based on adjusted values up to that range.

4.2.5 Empirical Adjustments for Non-Beam Filling

Equation (1) is in error when the radar beam is not filled with precipitation particles. The likelihood of intercepting a representative sample within the beam decreases as the distance to the target increases, because the radar beam widens and ascends above the surface of the earth as it travels away from the radar, until even the tallest storms will no longer fill the radar beam.

No satisfactory, explicit method exists for determining the degree of beam filling from individual radar measurements. It is possible, however, to derive statistics that give the average error caused by nonrepresentative beam sampling and non-beam filling (hereafter referred to as non-beam filling). This can be done by either (1) comparing radar with rain-gage data at various ranges, or (2) assuming that for radar data covering a sufficiently long period all unexpected variations with range, observed in the averages for that period, are the results of deficient beam filling.

Because no suitable rain-gage data existed for deriving the empirical adjustment, the second method was adopted for the analysis of the 5 days of undisturbed weather from June 22 through 26. This decision might be questioned because data were limited to such a brief period. This period was, however, free of convective disturbances, and the north-south variations were found to be approximately equal at all longitudes, indicating homogeneity in the east-west direction. An assumption implicit in the empirical procedure described below for applying non-beam filling adjustments is that there is east-west homogeneity in the average echo amount for the 5-day period. Figure 7 gives plots of the ratios of the mean echo area at radar ranges greater than 95 km to those at 95 km for a 65 km wide latitude band lying across the extreme southern portion of the BOMEX square. As the range increases from 95 km to 290 km, the shape of the curves for both radars similarly show rapid decreases in the mean echo amounts for the undisturbed period. These curves substantiate the assumption that there is east-west homogeneity in the mean 5-day echo amount.

For the moderately disturbed period on June 28 and 29, non-beam filling adjustments were not applied to the data. The size and height of the echoes accompanying the disturbance were quite large (fig. 4); therefore, the geometric features of the significant echoes are thought to be retained out to far radar ranges (see appendix). The curves in figure 7 for the disturbed period show that significant decreases in the mean echo amount do not exist until the range exceeds about 225 km.

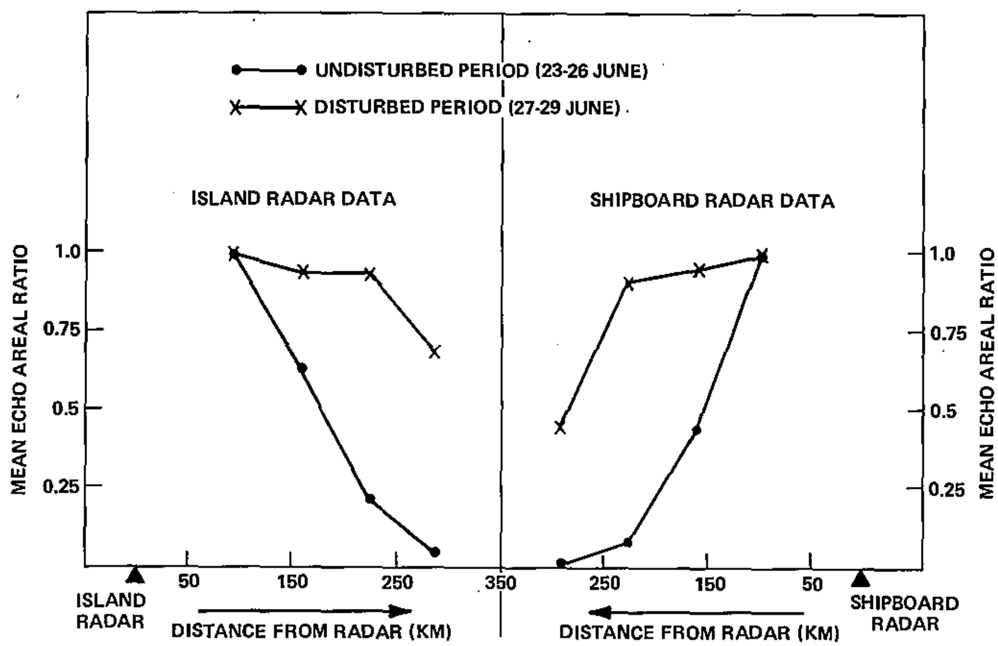

Figure 7.--Ratio of mean echo area at 95 km to that at further radar ranges for the undisturbed and disturbed periods.

As discussed by Hudlow (1970a), useful quantitative precipitation estimates are difficult to make by conventional procedures from the gain-step measurements for ranges beyond about 160 km. Quantitative estimates have been derived from BOMEX data for such ranges by means of the statistical echo model described in the appendix and the following step-by-step procedure, which, for the 5-day undisturbed period, incorporates an adjustment for non-beam filling:

(1) Calculate for each surface-based radar, from eq. (A-13) in the appendix and the census of echo lengths, the area-averaged rainfall rates for (a) areas inside the BOMEX box and within 160 km of the radar site, and (b) areas inside the BOMEX box but beyond 160 km of the radar.

(2) Compute within each radar umbrella the total precipitation deposited during the 5-day period over areas (a) and (b), based on the rainfall estimates derived above.

(3) Determine for each radar the ratio given by dividing the accumulated average precipitation for area (a) by the one for area (b) for the 5-day period.

(4) Adjust the rainfall estimates for individual time increments of 6 hr with these ratios under the assumption that they are approximately applicable to each 6-hr period within the 5 days.

For the 5-day period, the ratios between accumulated average precipitation for areas (a) and (b) were 5.5 for the island-based radar and 13.5 for the Discoverer radar. The standard deviations of the daily ratios from the 5-day mean ratios were 1.8 and 6.5 for the island and shipboard radars, respectively. The substantially larger ratio for the shipboard radar can partially be attributed to the combination of a larger beam width (1.25° compared with 1.0° for the island radar) and a shorter radar horizon resulting from the lower antenna height. The antenna for the shipboard radar was only about 20 m above mean sea level (m.s.l.), while the island radar was located about 290 m above m.s.l. (Hudlow, 1970a). The shipboard radar also suffered some beam losses from sea absorption and reflection, because it was operated normally at a 0° base antenna-tilt angle.

The probable maximum error induced into the precipitation estimates when following the procedure described here, including adjustments for non-beam filling, is presented in section 5.5.

4.3 Analysis of Satellite Data

Since no quantitative radar data were available for the northern 50 percent of the BOMEX box, satellite data were used to extrapolate the rainfall estimates for the southern half to the northern half. The fundamental supposition is that the ratios obtained by dividing the average cloud amounts over the southern half of the BOMEX box into those for the northern half, for each 6-hr interval, are equal to ratios based on average rainfall for the same areas and times.

Cloud amounts were estimated from satellite data, and since these data are available for the entire BOMEX box, the ratio discussed above derived from satellite cloud data provides a means of extrapolating rainfall estimates to the northern half of the box. Both visible and infrared data were used to estimate the cloud amounts. The infrared data provided one nighttime observation each night. Hudlow (1975) describes the procedure used to derive a normalization factor that relates the satellite image areas from the infrared data to equivalent areas from the visible data.

If the cloud types over the entire BOMEX area were reasonably homogeneous, then the ratios used in the rainfall extrapolation procedure should be realistic. In any case, since cloud amounts in the northern part of the BOMEX box were significantly smaller than in the southern, yielding extrapolations in a stable direction, and since 6-hr average ratios over large areas (50 percent of the BOMEX square) were used, the probable error resulting from this procedure should remain small. Martin and Scherer (1973) discuss the accuracy of satellite techniques for estimating rainfall.

5. DISCUSSION OF RESULTS

5.1 Echo-Rainfall Statistics Compared With Results Obtained by Other Investigators

In this section, comparisons are made between results from BOMEX and those from (1) an earlier radar investigation conducted in the vicinity of Barbados and (2) radar studies in the Miami, Fla., region. The latter comparison is considered pertinent since, according to most climatological classifications, Miami is in a tropical regime and has been used as a "testing ground" for certain sensors and techniques for the GARP Atlantic Tropical Experiment (GATE). GATE has objectives similar to those of BOMEX, but is an international effort broader in scope, aimed at covering a greater range of space and time scales during disturbed and undisturbed weather conditions.

Saunders (1965), who analyzed radar data for several echoes observed from Barbados, concluded from M-33 radar and island rain-gage data that rates in excess of 100 mm/hr at a point, sustained for as long as a few minutes, are not extremely rare. This compares favorably with the BOMEX radar data analysis. For example, from results based on the statistical echo model, described in the appendix, it can be shown that peak rainfall intensities of about 80 mm/hr at a point accompany an echo of size D = 55 km, the size echo that produces the greatest percentage of the rainfall. For an echo of this same size, the statistical model gives an average rainfall rate over the total echo area of about one-thirtieth that of the peak, or approximately 2.5 mm/hr. The echo area given by the statistical model for an echo 55 km in length is about 1,000 km^2. As shown later in this section, echo area depends on characteristics of the radar hardware; thus, the rainfall rate averaged over the total area of an echo will vary with the type of radar. This problem could be largely overcome if the echo areas were determined at a rain-rate threshold that the least sensitive radar could measure.

The statistical model yields a practical upper limit for instantaneous point rainfall rates of about 300 mm/hr for an echo 160 km in length, which corresponds to the largest echo observed during the June 28 and 29 disturbance. This result agrees favorably with the highest 1-min rain rates accompanying the drop-size distribution observed in Majuro, Marshall Islands, by Mueller and Sims (1969, p. 39). As explained in section 4.2.1, this drop-size distribution was adopted for the BOMEX analysis.

Figure 8 shows relative cumulative distributions, giving percentages of the total precipitation content within an echo that are distributed over given percents of the total echo area as derived from (1) the BOMEX radar analysis based on the statistical echo model and (2) the Miami radar analysis. The Miami curve (fig. 8) is based on points extracted from a curve presented by Woodley et al. (1971, p. 112), whose analysis was made using UM-10, 10-cm radar data for a few hundred convective clouds. The BOMEX curve almost envelops the upper points plotted on the scatter diagram used for fitting the Miami curve. This implies that the spatial gradients of liquid water were greater and/or that the cores occupied a smaller percent of the total echo area in the BOMEX than in the Miami radar echoes. However, part of the explanation for the difference between the BOMEX and Miami curves is due to differences in the characteristics of the two radars.

Both curves shown in figure 8 illustrate an important point: a large portion of the liquid water contained within an echo is distributed over a small portion of the echo area. Only 30 percent of the echo area contains 90 percent and 80 percent of the precipitation content for the BOMEX and Miami echoes, respectively. This result stresses the need for careful design of the meteorological sampling and the importance of collecting radar data in other large-scale experiments, such as GATE.

Woodley et al. (1972) and Martin and Scherer (1973) suggest that radar statistics can be used as calibration and transformation links for estimating rainfall from satellite data. One statistical relationship that could be used as a transformation function to relate satellite image data to rainfall estimates is a curve of rainfall amount versus echo area. Based on comparisons of radar and satellite patterns, a statistical regression relationship can be derived that relates selected features from the satellite pattern to an estimate of the equivalent radar echo area within the satellite cloud image. This estimated echo area is then used to find a rainfall estimate from the echo-area, rainfall curve.

Figure 9 shows a comparison of echo-area, rainfall curves derived from BOMEX and Miami radar data. The Miami curve is based on points extracted from a curve presented by Woodley et al. (1972, p. 21). The BOMEX curve, which was derived from the statistical echo model, was adjusted for differences in the characteristics of the MPS-34 and UM-10 radars. Byers (1948), who correlated echo area with rainfall from Florida thunderstorms, was one of the first to point out that the magnitude of echo area, as well as other geometric characteristics of echoes obtained from radar measurements, is dependent on the hardware characteristics of the radar. This is apparent from inspection of the radar equation (1), which shows that the power returned to the radar (signal strength) is a function of several hardware characteristics: P_t, G,

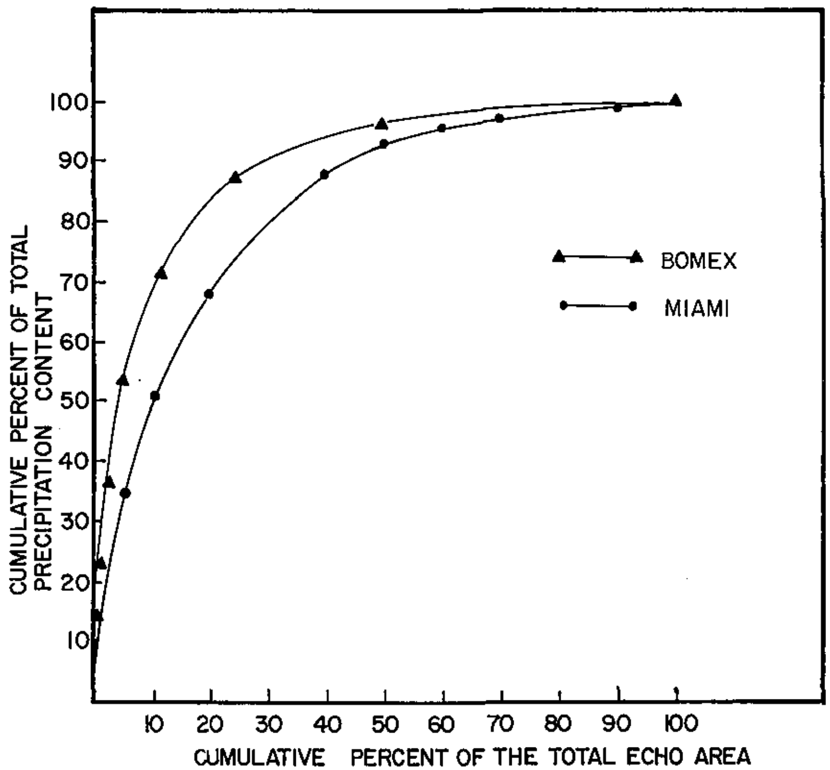

Figure 8.--Mean relative cumulative distributions of precipitation content for percentages of the total echo area for radar echoes observed in the BOMEX and Miami vicinities.

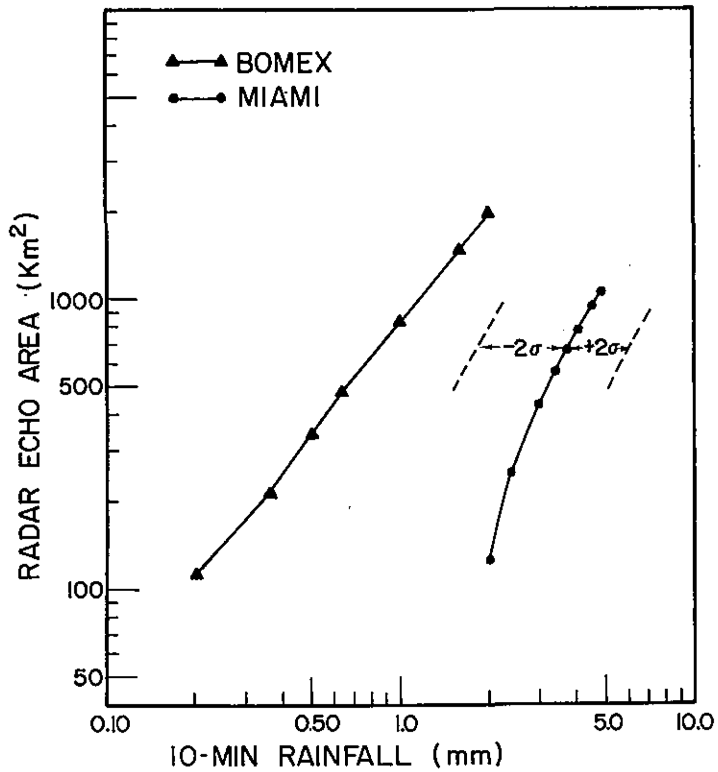

Figure 9.--Average 10-min rainfall over echo entities of various sizes (areas) for radar echoes observed in the BOMEX and Miami vicinities.

h, θ, and λ. Table 4 gives differences expressed as decibels for several factors that affect the sensitivity of the MPS-34 and UM-10 radars, the MPS-34 being the more sensitive of the two.

The difference between the radar constants of the two radars as shown in table 4 was derived by using a simplified formulation of the radar constant which includes only those parameters that vary with the radar characteristics. The difference formulation can be expressed as

$$\Delta(\mathrm{dB}) = 10\ \log\left[\frac{(P_t\tau/\lambda^2\theta^2)_{\mathrm{MPS-34}}}{(P_t\tau/\lambda^2\theta^2)_{\mathrm{UM-10}}}\right]$$
$$= 10\ \log\left[\frac{(180\mathrm{x}5\mathrm{x}10^{-6})/(3.2^2\mathrm{x}1^2)}{(450\mathrm{x}2\mathrm{x}10^{-6})/(10^2\mathrm{x}2^2)}\right] \simeq 16 \quad , \tag{7}$$

where P_t is the transmitted power, τ is the pulse duration (time units), λ is the wavelength, and θ is the beam width. The numerator and denominator terms are for the MPS-34 and UM-10 radars, respectively.

The difference in decibels shown in table 4 that stem from different normalization ranges is given by

$$\Delta(\mathrm{dB}) = 10\ \log\left(\frac{r_{10}}{r_{34}}\right)^2$$
$$= 10\ \log\left(\frac{185}{80}\right)^2 \approx 7 \quad , \tag{8}$$

where r_{10} and r_{34} are the normalization ranges in kilometers applied to the UM-10 and MPS-34 radar data, respectively.

By using eq. (A-1) in the appendix, it is possible to estimate the loss in echo area that would result from a reduction of 28 dB in the sensitivity of the MPS-34. Taking logarithms of both sides of eq. (A-1), multiplying through by 10, and solving for A_{eo} gives

$$A_{eo} = \frac{(\overline{P}_{ro} - \overline{P}_{rm})^2}{100b^2} \quad , \tag{9}$$

where A_{eo} is the echo area for maximum sensitivity (gain), and $\overline{P}_{ro}$ corresponds to the threshold power at the periphery of the echo. $\overline{P}_{ro}$ and $\overline{P}_{rm}$ are expressed in decibels with reference to 1 mW (dBm). Applying eq. (9), we can express the ratio of the echo area after the 28-dB reduction in sensitivity to the initial echo area as

$$\text{Areal ratio} = \frac{(77-\overline{P}_{rm})^2}{(105-\overline{P}_{rm})^2} \quad . \tag{10}$$

Table 4.--Differences between factors affecting the sensitivity of the MPS-34 and the UM-10 radars

Factor	Difference between MPS-34 and UM-10 radars (dB)
Minimum detectable signal of receiver	5
Radar constant	16
Range normalization	7
Total	28

Equation (10) was used for a series of echo sizes to derive the areal adjustments applied to the BOMEX curve in figure 9. Following these adjustments, the BOMEX curve differs by a factor of 4 from the Miami curve at the closest points (factor of 2 from the 2σ curve). Part of the explanation for this residual disagreement might be due to remaining unknown differences resulting from the dissimilar radar characteristics of the two radars or perhaps from intrinsic errors in the statistical model. Based on the error analysis presented in section 5.5, errors accompanying the X-band rainfall estimates, including those due to attenuation, are unlikely to be as large as a factor of 4. A logical conclusion is that there are significant differences between the BOMEX and Miami samples because of precipitation morphology. The Florida echoes are over land, and their structure is influenced by a convective regime forced by peninsula sea breezes, while the BOMEX echoes are for tropical oceanic convection in a trade-wind regime predominantly outside the intertropical convergence zone.

The curves in figure 9 are based on echo areas and rainfall amounts pertaining to echo entities. Implicit here is that the size (length) of an echo generally increases as the echo area increases. Figure 10 contains relative frequency histograms of echo lengths within 8 km class intervals for the disturbed and undisturbed periods of BOMEX Period III.

5.2 Space and Time Variations of Cloud and Echo Amounts

The time plots of cloud amounts derived from satellite data shown in figure 11 indicate consistently greater cloud coverage over the southern half, except at the very beginning of the period. The north-south differential in cloud amount is greatest during the 5 undisturbed days from June 22 through 26.

Both island and shipboard radar data were used in deriving figure 12, which shows the percent of areas within the BOMEX box covered by radar echo for 6-hr intervals during Period III. Non-beam filling adjustments were applied to the data for the 5-day undisturbed period by the empirical procedures described in section 4.2.5. The results in figure 12 do not reveal any east-west biases or differences that remain consistent throughout Period III. For the first 2 days of the period, a larger percent of echo coverage is observed with the island than with the ship radar, from which it can be inferred that echo amounts in the southwest quarter of the BOMEX box were larger than in

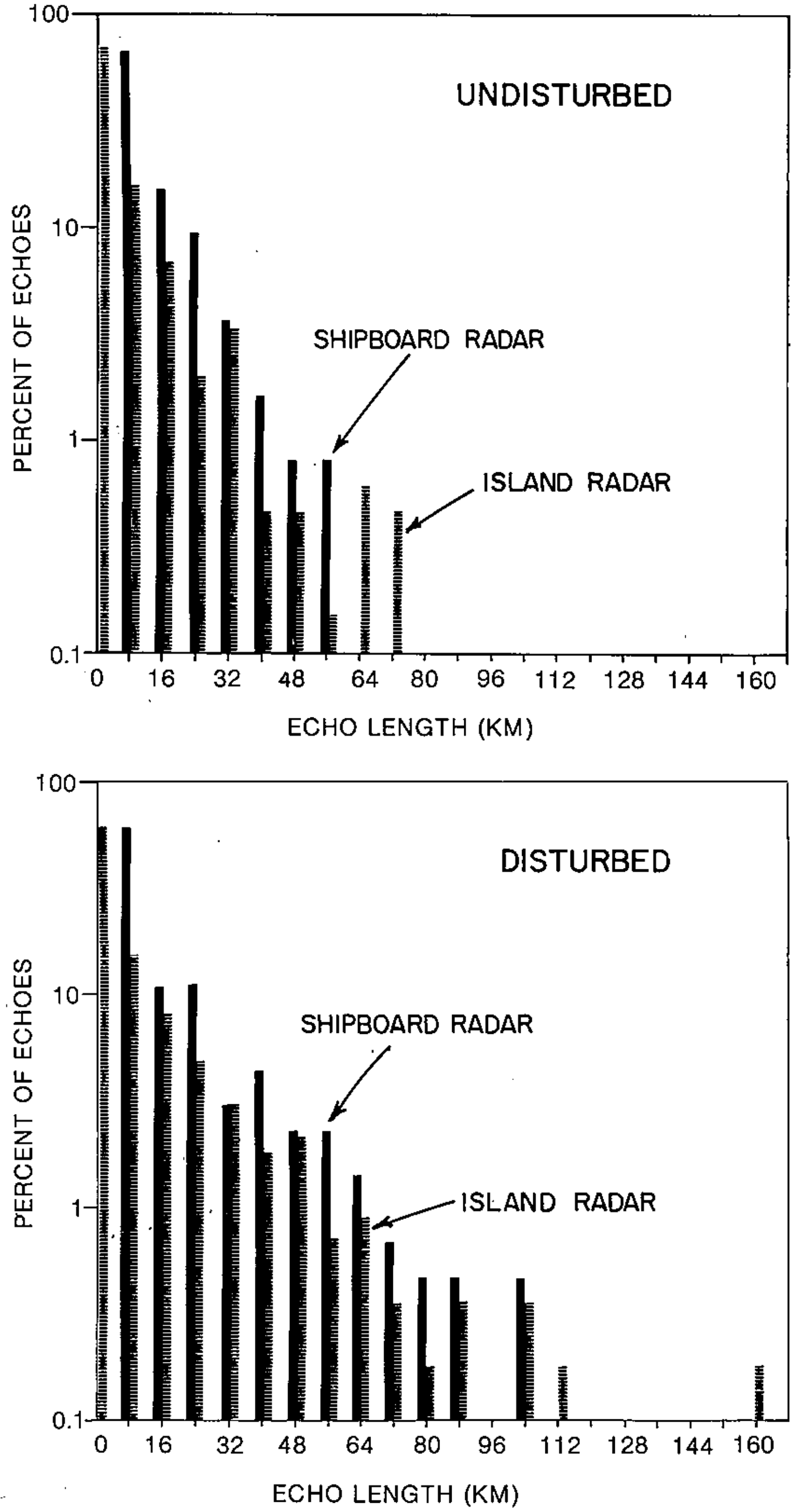

Figure 10.--Relative frequency histograms of echo lengths for the undisturbed and disturbed days of Period III.

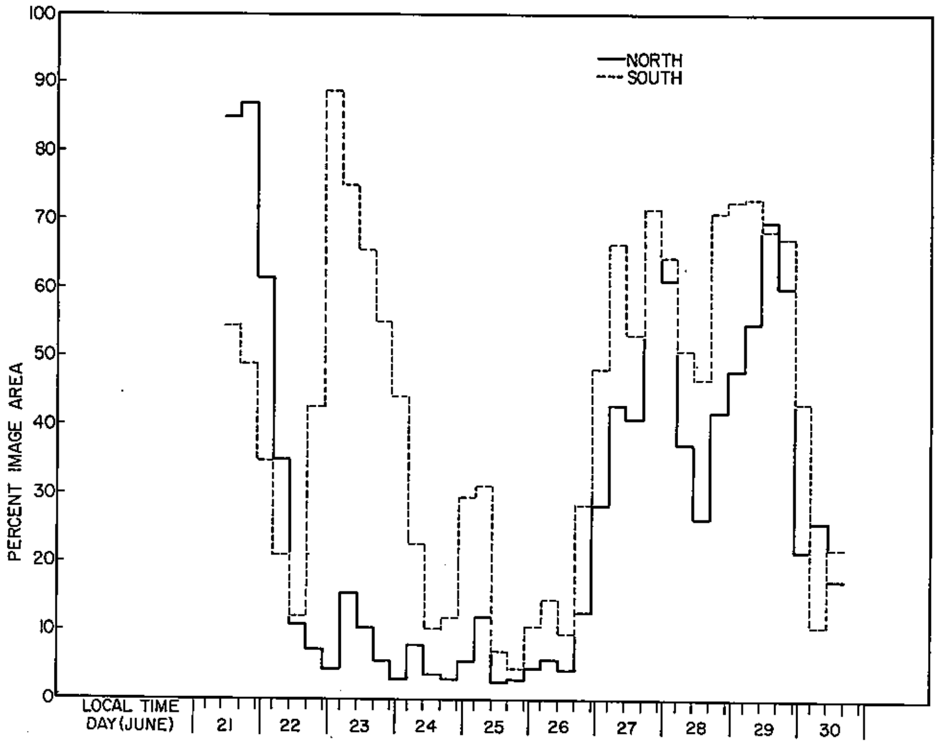

Figure 11.--Percent of the southern and northern halves of the BOMEX square covered by satellite cloud image during Period III.

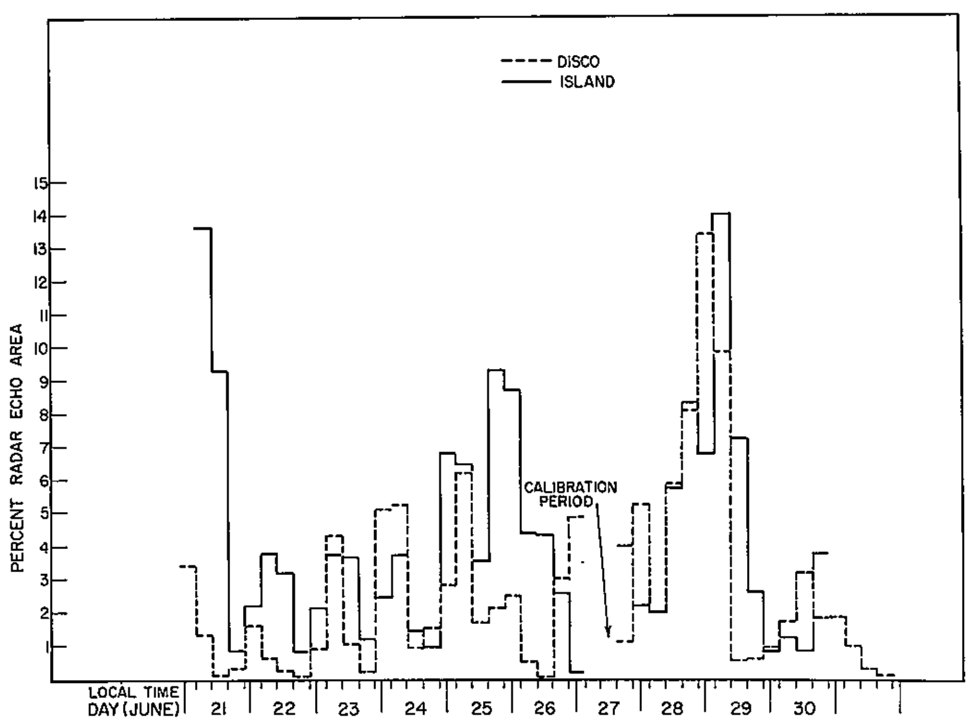

Figure 12.--Percent of those areas inside the BOMEX square out to radar ranges of 320 km which were covered by echo during Period III.

the southeast quarter during these 2 days. This finding correlates with the shipboard rain-gage measurements, which show that significant rainfall was recorded on June 22 (sec. 5.3) aboard the Mt. Mitchell at the southwest corner of the BOMEX square.

The comparatively large echo coverage observed by the island radar from midday of June 25 to midday on June 26 is the result of numerous small echoes rather than larger organized ones. Because echo size and rainfall are directly and nonlinearly related in this study through eq. (A-13) in the appendix, the rainfall estimates for the June 25 to 26 time period remain relatively low. Conversely, a few large echoes between 2200 l.t. on June 26 and 0400 l.t. on June 27 produced a measurable rainfall increase although there was not a proportional increase in total areal echo coverage.

Both the time plots of echo coverage presented here and the time plot of rainfall amount in section 5.4 show cyclic diurnal variations for the undisturbed days. Hudlow (1970a, 1970b, and 1975) has shown, using BOMEX radar data, that the mean diurnal variation of echo amount during undisturbed periods gives a maximum of echo activity around 0300 to 0400 l.t. and a broad minimum during the early afternoon hours. Hudlow (1970b) has further shown, based on a sample of 17 disturbed days, that mean diurnal variations in echo activity are not as pronounced for BOMEX disturbed conditions.

5.3 Shipboard Rain-Gage Analysis

The results of the analysis from the shipboard rain-gages are plotted in figure 13. These values are accumulated amounts for the 3 hr immediately preceding the abscissa times, and are shown as ratios relative to the values for June 21 from 1400 to 1700 l.t. Zeros and traces are omitted from the plot, and no data were missing except during the indicated calibration period.

The results from the rain-gage analysis support the description of the weather systems presented in section 3, revealing relatively quiescent conditions during practically the entire 5-day undisturbed period, with increases in convective rainfall just before and immediately after this period and with relatively disturbed conditions on June 28 and 29. Figure 13 also is quite consistent with the radar time plot of rain rate presented in section 5.4.

5.4 "Best Estimates" of Rainfall Amounts

The results from the quantitative precipitation analysis, as derived from radar and satellite data using the statistical echo model and other procedures outlined in section 4, are summarized by the bar graph in figure 14, showing average rainfall rates over the entire BOMEX box for 6-hr intervals. As seen in this figure, the average rainfall rate for the undisturbed period, June 22 through 26, is approximately 0.35 mm/day and the greatest 24-hr total, which is about equal on both June 25 and 26, is estimated at 0.5 mm. The average rate for the moderately disturbed period between 1000 l.t. on June 28 and 1600 l.t. on June 29 is approximately 5.5 mm/day, or more than an order of magnitude greater than during the undisturbed period. Daily rainfall estimates for each half of the BOMEX square as well as for the entire square are given in table 5.

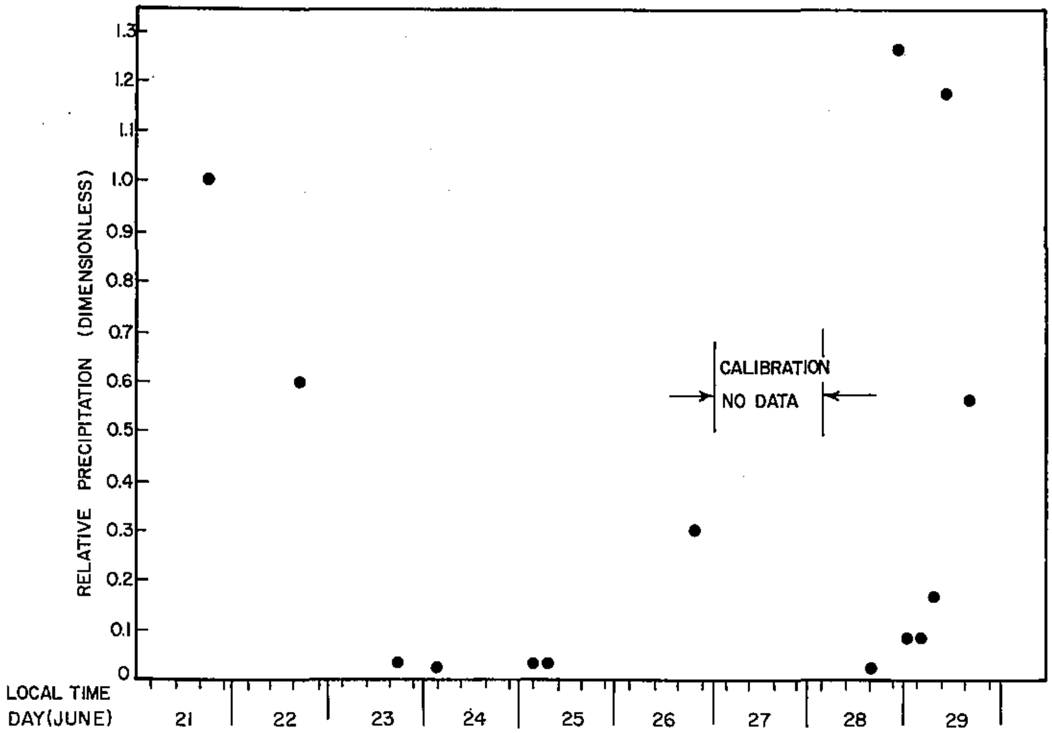

Figure 13.--Mean relative precipitation deposited over the BOMEX square during each 3-hr period of Period III as estimated from the five shipboard rain gages.

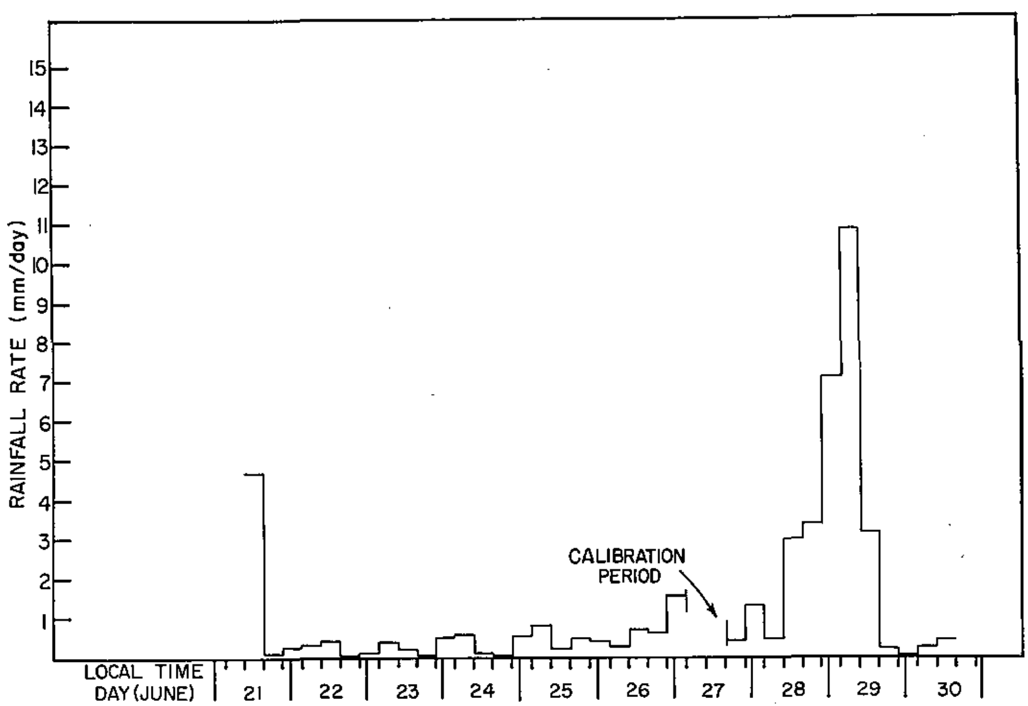

Figure 14.--Estimates of the average rainfall rate over the BOMEX square during Period III as derived from radar and satellite data.

Table 5.--Daily rainfall estimates for the BOMEX square

Date (1969)	Local time (l.t.)	Southern half (mm/day)	North/south satellite ratio	Northern half (mm/day)	BOMEX square (mm/day)
June 21-22	2200-2200	0.21	1.15	0.25	0.23
June 22-23	"	0.27	0.17	0.05	0.16
June 23-24	"	0.51	0.23	0.11	0.31
June 24-25	"	0.74	0.39	0.28	0.51
June 25-26	"	0.72	0.40	0.29	0.51
Calibration day					
June 27-28	2200-2200	2.48	0.65	1.61	2.05
June 28-29	"	5.93	0.80	4.70	5.32

Based on the above results and on the confidence limits discussed in section 5.5, and assuming that the evaporation rates do not exceed about 7 mm/day, it is concluded that the period from June 22 through 26 can be used for atmospheric water budget analysis with errors not exceeding 25 percent in the daily evaporation estimates and 12 percent in the estimate for the entire 5-day period. This finding does not necessarily apply to the disturbed period, since the rainfall estimates and the expected evaporation rates are comparable in magnitude, and the same percentage errors in the rainfall estimates can produce unacceptably large errors in the water budget analysis. These errors, and the consistency between the precipitation and water budget analysis, are examined more closely in the next two sections.

5.5 Probable Confidence Limits

The estimates given in the preceding section are subject to errors inherent in the rainfall derivations. Sufficient data are not available to precisely establish the magnitude of the errors, but based on results from other studies and by considering factors unique to BOMEX, it is possible to ascertain mean lower and upper confidence limits for the estimates.

From results reported by other investigators (e.g., Wilson, 1970; Borovikov et al., 1970), Hudlow (1975) concludes that if certain standard operational conditions are met, errors in radar estimates, on the average, can be held to less than a factor of 2. This finding applies to areal averages over a few hundred square kilometers and to integrated storm amounts of 1 mm or more. The following conditions give this degree of accuracy:

(1) Equipment capable of stable and reliable measurements.

(2) Suitable calibration, sampling, and processing procedures.

(3) Areas of measurement restricted to ranges of less than 150 km.

(4) Small rainfall attenuation.

(5) Seasonal adjustment applied to the radar data based on a comparison with drop-size and/or rain-gage data.

Thus, under optimum conditions the BOMEX radar estimates may be in error by a factor of 2, but the error may be greater because of specific circumstances surrounding the BOMEX radar program, which precluded strict adherence to all five conditions cited above. Potential additional sources of error for BOMEX are

(1) Attenuation by liquid water not accounted for with correction.

(2) Inaccuracy of the statistical echo model.

(3) Inadequacy of non-beam filling adjustments.

(4) Uncertainty from extrapolation via satellite data.

Hudlow (1975) uses variability and frequency analyses to estimate maximum additional error that may arise from these four sources. Since the quality and completeness of the radar coverage is not the same for all portions of the BOMEX area, the error analysis was stratified as listed in table 6. Figure 15 shows the relative fraction of the BOMEX area covered by radar at ranges of less than 160 km ($A_1 + A_2$) and greater than 160 km ($A_3 + A_4$), and by satellite only (A_5).

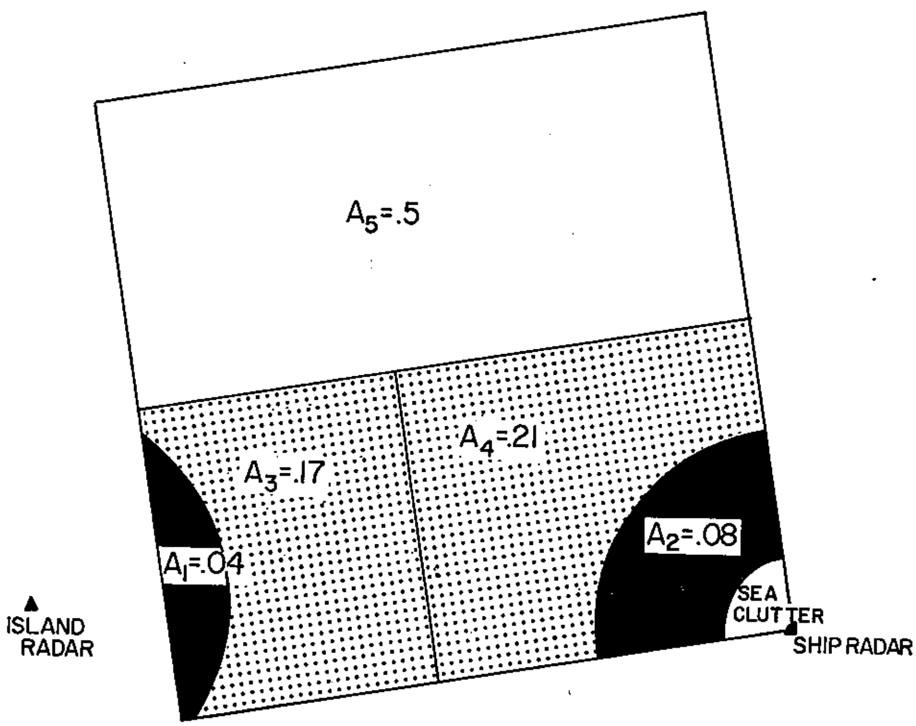

Figure 15.--Schematic illustrating the portions of the BOMEX square covered with radar measurements, for ranges inside and outside 160 km, and the portion covered only by satellite measurements.

Table 6.--Summary of confidence limits for radar rainfall estimates, expressed as error factors

Subsections of BOMEX area	Average confidence limits under "standard operational conditions"	Upper limits for BOMEX conditions	
		Daily	5-day undisturbed and 2-day disturbed periods
Less than 160 km radar range	2.0	2.4	2.0
Southern half	2.0	3.3	2.0
Entire BOMEX square	2.0	5.0	2.5

The numbers in table 6 give the average error (2.0) under the standard conditions described above, and the error that, in the worst case, can accompany the daily and period estimates for various portions of the BOMEX square. For example, daily rainfall estimates for the southern half of the area are expected to be in error, on the average, by a factor of 2.0. The estimate for a specific day could be in error by a greater or lesser amount, but should not exceed a factor of 3.3 for the estimates over the southern half.

As seen in table 6, the probable upper limit of the error is higher for the daily estimates than for the entire period, primarily because the underlying assumption in the procedure used to adjust for non-beam filling (sec. 4.2.5) is less valid for shorter time periods. The reason for the markedly higher upper limit for the entire BOMEX square compared with the southern half lies in potential errors associated with the procedure for using satellite data (sec. 4.3) to extrapolate the radar coverage over the southern half of the BOMEX square to the northern half. The relative error is the same for both disturbed and undisturbed periods, although one might expect a higher upper limit for the disturbed period since errors stemming from liquid-water attenuation can increase with greater rainfall rates. However, as discussed by Hudlow (1975), relative errors from other sources (especially non-beam filling) decrease during the disturbed period, compensating for the increase in error caused by liquid-water attenuation.

The base error factor of 2.0 applies, as stated earlier, to areal averages over a few hundred square kilometers. The fact that the BOMEX analysis covers an area thousands of square kilometers may, therefore, lower this factor.

5.6 Comparison of Precipitation and Atmospheric Water Budget Analyses

Although the confidence limits discussed in the preceding section are based on a logical but somewhat discretionary analysis scheme, the true error in any of the estimates should not exceed the upper limit given in table 6. It may be less, but how much less can be determined only by comparison with independent data.

One of the principal reasons for deriving the quantitative precipitation estimates given in section 5.4 is to assess the precipitation term in the water budget equation (Rasmusson, 1975), making it possible to solve for evaporation from the ocean surface. In another application of the budget equation, precipitation can be derived by independently estimating evaporation from a bulk aerodynamic equation. Some of Rasmusson's results are shown in table 7, where E is evaporation, P is precipitation, and C_q is the drag coefficient used in the aerodynamic model.

Table 7.--Comparison of water budget residuals and precipitation estimates

Term	Derivation method	5-day undisturbed period (mm/day)	2-day disturbed period (mm/day)
(E-P)	Budget residual: assume $F_{M500}=0$	7.1	3.7
E	Bulk aerodynamic: assume $C_q=1.24\times10^{-3}$	7.4	7.7
P	Budget analysis	0.3	4.0
P	Radar-satellite analysis	0.3	3.7

As seen in table 7, there is excellent agreement between the precipitation estimates obtained by the budget and radar-satellite analyses. As Rasmusson points out, the validity of the assumption $F_{M500} = 0$ (zero subgrid-scale flux in water substance through the top of the BOMEX box) becomes questionable during disturbed periods. Since it is also expected that the absolute magnitude of the error in the radar-satellite estimates will increase under disturbed conditions, the good agreement shown in table 7 may be coincidental, but, in view of the results presented in this report and those discussed by Rasmusson, it is likely that the error contained in the rainfall estimate derived from the radar-satellite analysis for the disturbed period is significantly less than the upper limit given in table 6.

6. CONCLUDING REMARKS

Radar, satellite, and rain-gage data have been used in describing the precipitation morphology for 5 undisturbed days (June 22 through 26) and 2 moderately disturbed days (June 28 and 29) during BOMEX Observation Period III. The average cloud and echo amounts were found to decrease with increasing latitude. No mean east-west variability was detected. Estimated average rainfall over the BOMEX square during the entire undisturbed period was ~0.35 mm/day, with the largest 24-hr total (on both June 25 and 26) being 0.5 mm. The average precipitation rate for a 30-hr disturbed period on June 28 and 29 was ~5.5 mm/day, or more than an order of magnitude higher than during undisturbed conditions.

Based on the small magnitudes of precipitation during the 5 undisturbed days, considering the confidence limits placed on the rainfall estimates (sec. 5.5), and assuming the evaporation rate does not exceed ~ 7 mm/day, we can conclude that the undisturbed period from June 22 to 26 can be used for atmospheric budget analysis, with errors in the evaporation estimates, which originate from errors in the estimated precipitation, not exceeding 25 percent in the daily estimates and 12 percent in the estimate for the entire period. Since the rainfall and expected evaporation rates are comparable in magnitude for the disturbed conditions on June 28 and 29, the maximum absolute error in the rainfall estimates, as given in table 6, could produce unacceptably large errors in the water budget analysis. However, from independent evaporation estimates computed with the bulk aerodynamic model and from precipitation derived from the budget residual, one can conclude that the error in the precipitation estimate for the disturbed 2-day period must be relatively small compared with the confidence limits given in table 6.

In addition to their application in precipitation computations for atmospheric budget analysis, the BOMEX radar data have been used here for several statistical studies. Conclusions drawn from these studies, some of which are significant for the planning of further tropical experiments, include the following:

(1) The echo-area and rain-rate time plots for undisturbed days show cyclic diurnal variations with maximum echo activity often observed around 0300 to 0400 l.t. and a minimum during the early afternoon hours.

(2) Much of the liquid water (80 to 90 percent) contained within a tropical convective echo at an instant in time is distributed over a small portion of the echo area (30 percent). This finding stresses the necessity for careful design of meteorological sampling and the importance of good radar coverage in tropical oceanic experiments.

(3) The average precipitation accompanying tropical convective echoes is highly correlated with the size (length) of the echoes. Since echo area is directly related to echo length, rainfall amount is proportional to echo area.

(4) Caution must be exercised in using empirically derived transfer functions to relate rainfall rate to the geometric characteristics of the echo, since the empirical relationship may change significantly with different sensors and under different meteorological conditions. The relationship should be derived for echo entities bound by a rain-rate threshold that is detectable by the various sensors. If this is not possible, a technique like the one described in section 5.1 can be used as a first approximation to adjust for effective changes in sensor sensitivity. When this technique was used to normalize for dissimilar system characteristics between the BOMEX MPS-34 and the Miami UM-10 radars, a large offset remained between the rain-rate, echo-area curves. This is not too surprising, since the convection morphology in the two areas may differ appreciably, but it does emphasize that a transfer function derived for use with, for example, satellite rain-rate techniques should be verified with radar data collected during the same time span and within the same locality.

The greatest deficiency in the BOMEX precipitation analysis stems from the incomplete coverage of the BOMEX square by quantitative radar measurements. This deficiency was partly overcome at the expense of increasing the probable error of the estimates, through extension of the radar data to far ranges by using a statistical model of radar echoes and an empirical adjustment for non-beam filling, and by using satellite data to extrapolate over areas not covered by radar. In subsequent tropical experiments, the complete experimental area should be covered with quantitative radar measurements. Ideally, the radar network should consist of radars with 5-cm or longer wavelengths and 1.75° or smaller beam widths. A sufficient number of radars should be available to cover the experimental area, with the radars spaced no further apart than about 175 km.

ACKNOWLEDGEMENTS

The authors are grateful to Joshua Z. Holland and Vance A. Myers for overall direction in the preparation of this study, to Eugene M. Rasmusson for providing results from the atmospheric water budget analysis and for his review of the manuscript, and to Jason K. S. Ching for the evaporation estimates from the bulk aerodynamic computations. Considerable help in basic data reduction was provided by Briah Connor. Thanks are also due Michael Divilio and Bryce Winn, who participated in the computer programming.

Satellite data were furnished by the Photographic Laboratory, Nimbus and ATS Data Utilization Center, Goddard Space Flight Center, NASA.

APPENDIX

Statistical Model of Precipitation Echoes

Background and Objective

A quantitative statistical model that describes the vertical extent, the horizontal intensity distribution, and the areal coverage of a radar echo, using a one-dimensional geometric parameter of the echo as the independent variable, has been developed from BOMEX radar data (Hudlow, 1971). The model provides a method for deriving precipitation estimates for the BOMEX box for areas and times when only maximum gain data (no gain-stepping) are available. It can also be used for deriving quantitative precipitation estimates at ranges exceeding 160 km from the BOMEX radars, ranges for which meaningful gain-step measurements are unlikely (Hudlow, 1970a). Only 12 percent of the BOMEX experimental area was covered by radar measurements at these ranges (fig. 15, sec. 5.5)

The validity of applying the echo model to extend the useful range of the BOMEX radar data can be inferred from the mean profiles of echo area versus height shown in figure A-1. The three vertical profiles correspond to three classes of echoes: (1) echoes less than 15 km in length, (2) echoes between 15 km and 30 km in length, and (3) echoes with lengths exceeding 30 km. The mean profiles illustrate that echo area, and thus echo length, tends to remain essentially constant with altitude in the lower troposphere, as is also shown by mean reflectivity profiles for intense New England thunderstorms presented by Donaldson (1961).

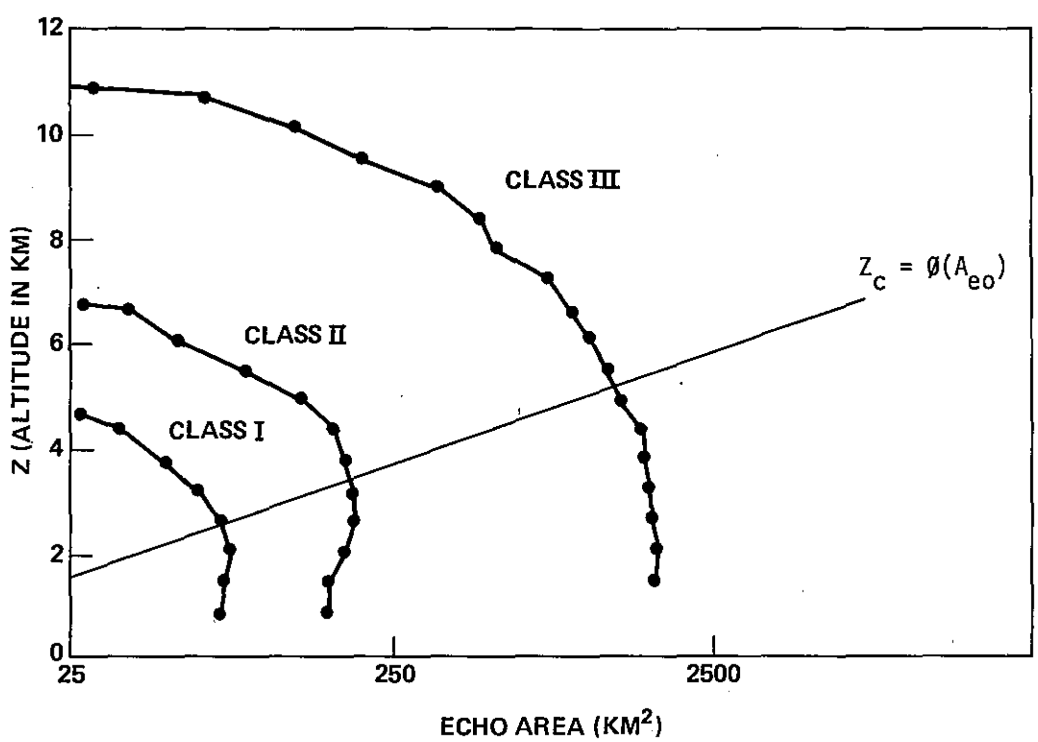

Figure A-1.--Average profiles depicting echo area versus altitude above sea surface for three classes of echo sizes.

If the area of an echo is greater than any abscissa value given in figure A-1, the supposition that representative measurements of the echo area or length can be made up to beam altitudes given by Z_c is justified, e.g., 2,600 km^2 for Z = 6.0 km. Assuming standard atmospheric refraction and a base antenna-tilt angle of 0°, the center of the radar beam is 6 km above the surface of the earth at a range of 320 km.

As shown later, the maximum dimension (length) of a radar echo, recorded at the base-tilt angle, constitutes a significant estimate of other echo parameters. Kessler (1965) recognized the importance of radar echo statistics for parameterizing the morphology of mesoscale precipitation, and stresses echo length as an important statistic.

Echo length was selected as the independent variable in the regression equations presented below and a computer algorithm was designed to scan digital radar data and estimate the length of each radar echo. An alternate choice would have been to use echo area as the independent variable, since a highly significant correlation exists between echo area and echo length for the BOMEX data set.

Data Analysis

Sixty-two radar echoes make up the statistical sample selected from data collected on May 29, during 7 days in June, and on July 1, 1969. The 62 echoes were all observed within 150 km of the radar site (average range to echo centroids = 100 km), with echo sizes varying in length from 6.5 km to 250 km.

The echo parameters for the sample were derived manually from photographic prints using grid overlay and graphical techniques. Echo entities were identified as consisting of continuous echo area (no breaks).

The maximum power returned to the radar from the intensity peak within an echo, $\overline{P}_{rm}$, was estimated by plotting the power corresponding to each gain threshold (in dBm) versus the square root of the echo area persisting at that threshold and extrapolating a straight-line relationship to zero area. When the value for $\overline{P}_{rm}$ derived in this manner exceeded a threshold setting of power for which echo was not observed to persist, it was assumed equal to the threshold setting. Corrections were made for range attenuation ($1/r^2$) and for atmospheric and rainfall attenuations (sec. 4.2.4).

The altitude of echo summits and the echo area at specific altitudes were derived from sequences of data collected at several antenna-tilt angles, spaced at 1/2° increments; corrections for earth curvature, beam width, and standard atmospheric refraction were applied. Constant-altitude plan views were manually constructed by superimposing finite range increments from photographs taken at several antenna-tilt angles.

Conventional least-squares techniques were used in the regression analyses. Geometric and exponential models were selected, and frequency histograms of the logarithmically transformed variables were examined for normality. Chi-square and Cornu tests for normality were run on the logarithm of echo lengths and the maximum powers (in dBm). The null hypothesis of normality was accepted for both distributions.

Mathematical Development

An exponential expression relating the spatial distribution of power returned from an echo to the length of the echo was formulated. The exponential model relates threshold received power, $\overline{P}_{ri}$, to the square root of the echo area, $\sqrt{A_{ei}}$, persisting at gain threshold i,

$$\overline{P}_{ri} = \overline{P}_{rm}\, 10^{-b\sqrt{A_{ei}}} \quad . \tag{A-1}$$

The intercept, $\overline{P}_{rm}$, and slope, b, are found to correlate closely with echo length. Equation (A-1) is illustrated in figure A-2, which, in hydrologic terminology, can be referred to as a depth-area curve.

Equation (A-1) is similar to echo models reported by several other investigators (e.g., Holtz, 1968; Altman, 1970). Huff (1968), using rain-gage data from a 1,000-km^2 network, concluded that a logarithmic square-root relationship frequently approximates the depth-area distribution of storm precipitation for storms of short duration. While the functional form of eq. (A-1) can be shown to hold for a wide variety of convective conditions, the $\overline{P}_{rm}$ and b coefficients will not only vary as a function of echo size, but may vary for a given echo with stage of development, synoptic conditions, geographic location, and radar characteristics.

Least-squares analyses gave the following regression equations:

$$\overline{P}_{rm} = 5.63\times10^{-8}D^{1.58} \quad , \quad \rho = 0.71 \quad , \tag{A-2}$$

$$b = 3.75D^{-0.79} \quad , \quad \rho = 0.94 \quad , \tag{A-3}$$

$$A_{eo} \doteq 2.95D^{1.44} \quad , \quad \rho = 0.95 \quad , \tag{A-4}$$

$$h = 5.88 \log_{10}D-1.56, \quad \rho = 0.84 \quad , \tag{A-5}$$

where D is the echo length (km), A_{eo} is the echo area (km^2) at the maximum receiver gain setting, h is the summit height of an echo (km), and ρ is the correlation coefficient.

From eqs. (3) and (4), and using the MPS-34 radar constant and normalizing to a range of 80 km, we obtain

$$R = 1.802\times10^{5}(\overline{P}_r)^{0.745} \quad , \tag{A-6}$$

where R is rainfall rate (mm/hr) and $\overline{P}_r$ is returned power (mW). Substituting (A-2) for $\overline{P}_r$ in (A-6) gives

$$R_m = 0.72D^{1.18} \quad , \tag{A-7}$$

where R_m is the maximum point instantaneous rainfall rate (mm/hr) within an echo.

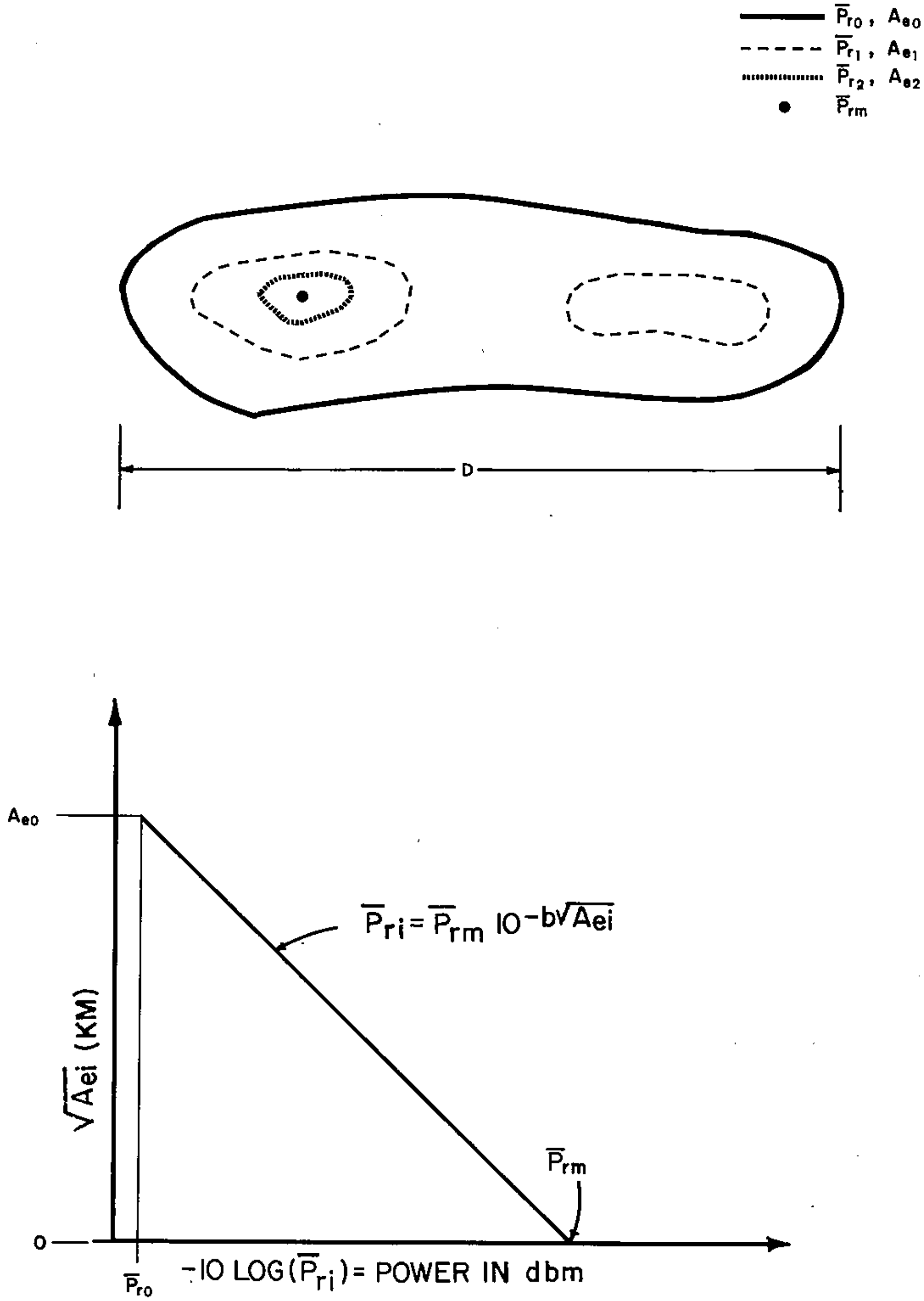

Figure A-2.--Hypothetical schematic of multicore radar echo with length D (top). Hypothetical plot of the square root of the radar echo area persisting at a threshold, i, versus the threshold power measured by the radar (bottom).

The rainfall rate averaged over a horizontal slice through a radar echo is given by

$$\overline{R}_e = \int_{\overline{A}_{eo}}^{o} R \, dA_e \Big/ \int_{\overline{A}_{eo}}^{o} dA_e \quad . \tag{A-8}$$

Substituting (A-6) and (A-1) in (A-8) gives

$$\overline{R}_e = 1.802 \mathrm{x} 10^5 \int_{A_{eo}}^{o} \overline{P}_{rm}^{\,0.745} \, 10^{-0.745b\sqrt{A_e}} \, dA_e \Big/ \int_{A_{eo}}^{o} dA_e \quad . \tag{A-9}$$

Analytical integration of (A-9) yields

$$\overline{R}_e = \frac{2.1 \mathrm{x} 10^5 \, \overline{P}_{rm}^{\,0.745}}{bA_{eo}} \left[\frac{0.583}{b} \left(1 - 10^{-0.745b\sqrt{A_{eo}}} \right) - \sqrt{A_{eo}} \cdot 10^{-0.745b\sqrt{A_{eo}}} \right] \quad . \tag{A-10}$$

Equation (A-10) can be reduced to a geometric function by plotting solutions for $\overline{R}_e$ for various D's as a straight line on logarithmic paper. The resulting equation is

$$\overline{R}_e = 0.013D^{1.31} \quad , \tag{A-11}$$

which gives the rainfall rate averaged over the area of an echo in mm/hr. The rate of rainfall averaged over any geometric area is given by

$$\overline{R} = \left(\sum_{j=1}^{N} \overline{R}_{e(j)} \, A_{eo(j)} \right) \Big/ A \quad , \tag{A-12}$$

where N is the number of echoes in the area, A. Substituting (A-4) and (A-11) into (A-12) gives

$$\overline{R} = \left(0.038 \sum_{j=1}^{N} D_j^{\,2.75} \right) \Big/ A \quad . \tag{A-13}$$

Equation (A-13) is for an instant in time, and the effect of echo duration as a function of echo size is not considered. The 2.75 exponent is reasonably close to what one would expect, for example, for hemispherical or cylindrical echoes with homogenous liquid-water concentrations and mean vertical velocities that are linearly proportional to the heights of the echo summits.

Model Tests

Equations (A-4), (A-11), and (A-12), which are the ones used in deriving the rainfall estimates presented in section 5.4, were tested by comparing these estimates to those obtained directly from digitized gain-step data. Independent verification of the model could best have been accomplished by comparison with Barbados rain-gage data. This was not feasible because the extent of the sea-land clutter prevented observation of entire echo entities at ranges closer than about 50 km. Using gain-step data for model verification is considered adequate, since an overall calibration was derived by comparing radar rainfall estimated directly from gain-step data to Barbados rain-gage data (sec. 4.2.2).

In figures A-3 and A-4, the model estimates of echo area and rainfall rate are compared with those obtained directly from the digitized gain-step data for 12-hr undisturbed periods on June 22 and 26. The areal estimates are instantaneous, while the rain-rate estimates are 6-hr averages, and both are for a 7,750-km^2 area within 150 km of the island radar. Figures A-5 and A-6 are analogous to figures A-3 and A-4, except that they are for a moderately disturbed period on June 29 and for a 30,000-km^2 area.

Figures A-3 and A-5 show that the model estimates of echo area will result in negligible errors for 6-hr averages. The average difference in the 6-hourly rain rates from the statistical model and the digitized gain-step data, shown in figures A-4 and A-6, is about 30 percent.

Table A-1 contains comparisons of the echo areas from shipboard radar data inside the BOMEX square based on (a) eq. (A-4) and (b) areal integration from digitized data. The 6-hr periods on June 23 and 26 are for undisturbed weather conditions; the periods on June 28 and 29, for moderately disturbed activity. The percent difference between the estimates from the model and the digitized gain-step data is consistently small, which justifies use of the model, developed from the island radar data, with the shipboard radar data.

Table A-1.--Estimates of echo areal coverage from shipboard radar data

Date	Local time	Area (km^2) (a) model	Area (km^2) (b) observed	Percent difference $\|(o - m)/o\| \times 100$
June 23	0200-0800	559.24	672.85	16.9
June 26	0800-1400	72.35	89.68	19.3
June 28	0200-0800	4,110.41	5,030.94	18.3
June 29	0200-0800	12,154.47	10,446.82	16.3

Although errors accompanying the use of eq. (A-13) can be large for an instant in time, its use with BOMEX radar data is adequate for purposes of this study, since the integration time is long and the area, A, is large.

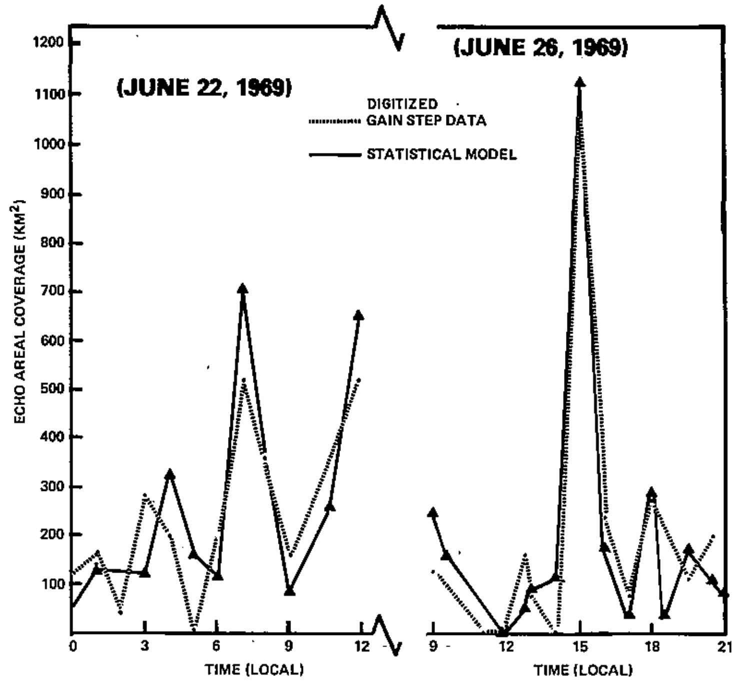

Figure A-3.--Echo areal coverage derived from the statistical model compared with that computed directly from the digitized gain-step data for two undisturbed periods.

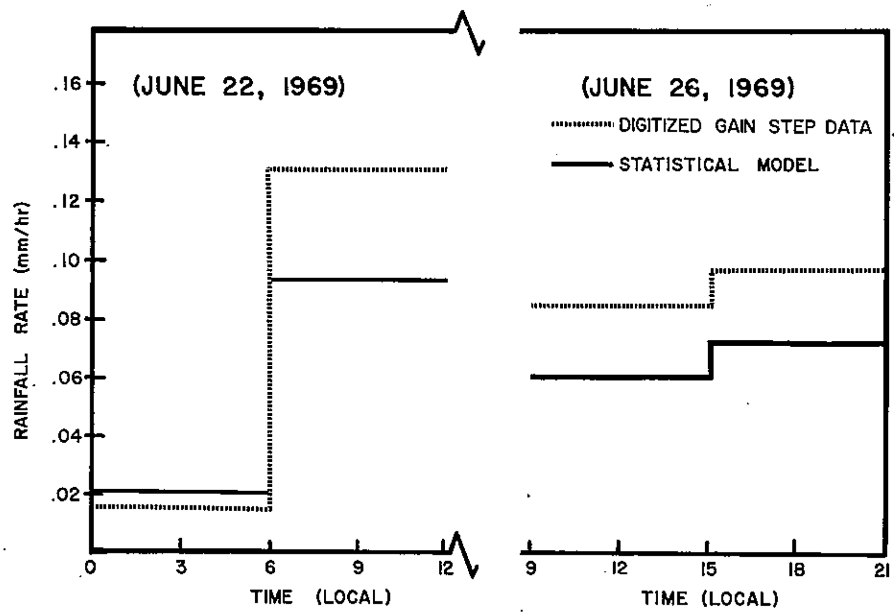

Figure A-4.--Average rainfall rates over a 7,750-km^2 area for 6-hr intervals derived from the statistical model compared to those computed directly from the digitized gain-step data for two undisturbed periods.

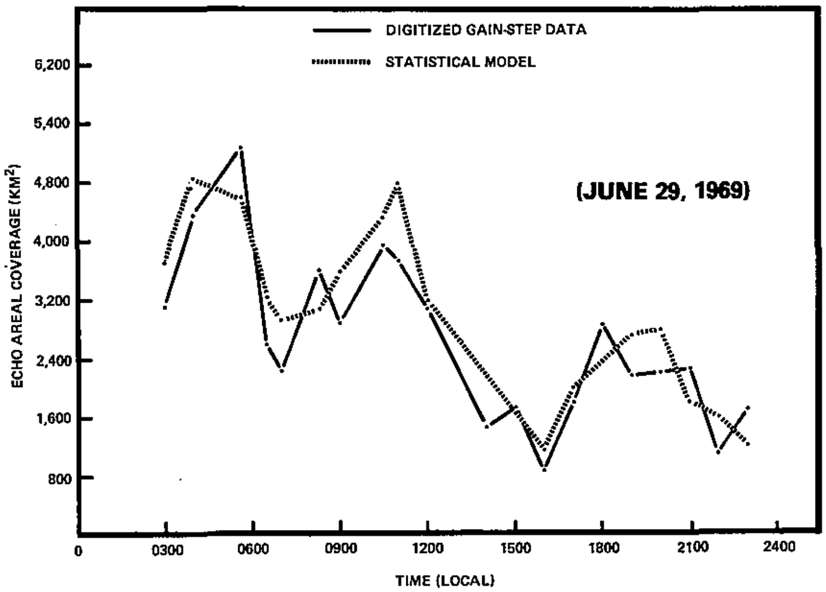

Figure A-5.--Echo areal coverage derived from the statistical model compared with that computed directly from the digitized gain-step data for a disturbed period.

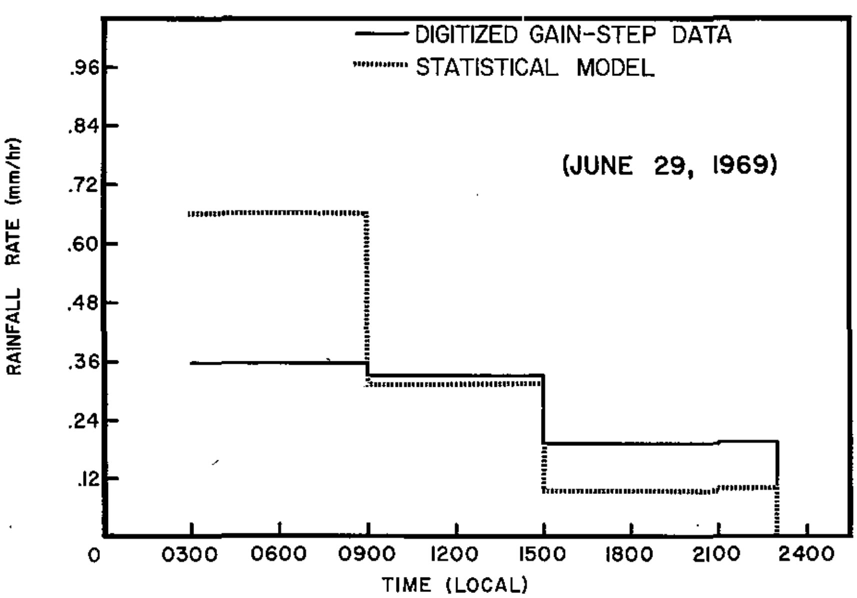

Figure A-6.--Average rainfall rates over a 30,000-km^2 area for 6-hr intervals derived from the statistical model compared to those computed directly from the digitized gain-step data for a disturbed period.

REFERENCES

Altman, F. J., "Storm Reflectivity Models," Preprints for 14th Radar Meteorology Conference, American Meteorological Society, November 1970, pp. 291-295.

BOMAP Office, BOMEX Field Observations and Basic Data Inventory, National Oceanic and Atmospheric Administration, U.S. Department of Commerce, Rockville, Md., March 1971, 428 pp.

BOMAP Office, "BOMEX Permanent Archive: Description of Data," NOAA Technical Report EDS 12, National Oceanic and Atmospheric Administration, U.S. Department of Commerce, Washington, D.C., May 1975, 327 pp.

Borovikov, A.M., V.V. Kostarev, I.P. Mazin, V.I. Smirnov, and A.A. Chernikov, Radar Measurement of Precipitation Rate, Israeli Translation from Russian, U.S. Department of Commerce Clearinghouse for Federal Scientific and Technical Information, Springfield, Va., 1970, 112 pp.

Byers, H. R., "The Use of Radar in Determining the Amount of Rain Falling Over a Small Area," Transactions of the American Geophysical Union, Vol. 29, No. 2, 1948, pp. 187-196.

Donaldson, R. J., Jr., "Radar Reflectivity Profiles in Thunderstorms," Journal of Meteorology, Vol. 18, No. 3, June 1961, pp. 292-305.

Frank, Neil L., "Atlantic Tropical Systems of 1969," Monthly Weather Review, Vol. 98, No. 4, April 1970, pp. 307-314.

Hitschfeld, Walter, and Jack Bordan, "Errors Inherent in the Radar Measurement of Rainfall at Attenuating Wavelengths," Journal of Meteorology, Vol. 11, No. 1, 1954, pp. 58-67.

Holland, Joshua Z., "Preliminary Report on the BOMEX Sea-Air Interaction Program," Bulletin of the American Meteorological Society, Vol. 51, No. 9, September 1970, pp. 809-820.

Holland, Joshua Z., "The BOMEX Sea-Air Interaction Program: Background and Results to Date," NOAA Technical Memorandum ERL BOMAP-9, Center for Experiment Design and Data Analysis, U.S. Department of Commerce, Rockville, Md., March 1972a, 34 pp.

Holland, Joshua Z., "Comparative Evaluation of Some BOMEX Measurements of Sea Surface Evaporation, Energy Flux and Stress," Journal of Physical Oceanography, Vol. 2, No. 4, October 1972b, pp. 476-486.

Holland, Joshua Z., and Eugene M. Rasmusson, "Measurements of the Atmospheric Mass, Energy, and Momentum Budgets Over a 500-Kilometer Square of the Tropical Ocean," Monthly Weather Review, Vol 101, No. 1, January 1973, pp. 44-55.

Holtz, C. D., "A Model of the Distribution of Precipitation in Three Dimensions," Proceedings of the 13th Radar Meteorology Conference, American Meteorological Society, August 1968, pp. 110-113.

Hudlow, Michael D., "Weather Radar Investigations on the BOMEX," Research and Development Report, ECOM-3320, U.S. Army Electronics Command, Ft. Monmouth, N.J. (available from DDC or NTIS), September 1970a 106 pp.

Hudlow, Michael D., "Radar Echo Climatology East of Barbados Derived from Data Collected During BOMEX," Preprints for 14th Radar Meteorology Conference, American Meteorological Society, November 1970b, pp. 433-437.

Hudlow, Michael D., "Three-Dimensional Model of Precipitation Echoes for X-Band Radar Data Collected During BOMEX," BOMEX Bulletin No. 10, BOMAP Office, National Oceanic and Atmospheric Administration, U.S. Department of Commerce, Rockville, Md., June 1971, pp. 51-63.

Hudlow, Michael D., "Radar and Satellite Precipitation Analysis of a 5-Day BOMEX Data Sample," NOAA Technical Memorandum, 1975 (In preparation).

Huff, F. A., "Spatial Distribution of Heavy Storm Rainfall in Illinois," Water Resources Research, Vol. 4, No. 1, 1968, pp. 47-54.

Jones, R. F., And S. G. Bigler, (Chairmen), "Use of Ground-Based Radar in Meteorology," World Meteorological Organization Technical Note No. 78, WMO-No. 193, TP. 99, 1966, pp. 11-13.

Kessler, E., "Computer Program for Calculating Average Lengths of Weather Echoes and Pattern Bandedness," Technical Note 3-NSSL-24, National Severe Storms Laboratory, Norman, Oklahoma, 1965, pp. 99-110.

Martin, David W., and Wolfgang D. Scherer, "Review of Satellite Rainfall Estimation Methods," Bulletin of the American Meteorological Society, Vol. 54, No. 7, July 1973, pp. 661-674.

Myers, Vance A., BOMEX Atlas of Satellite Cloud Photographs, BOMAP Office, National Oceanic and Atmospheric Administration, U.S. Department of Commerce, Rockville, Md., July 1971, 250 pp.

Mueller, E. A., and A. L. Sims, "Relationships Between Reflectivity, Attenuation, and Rainfall Rate Derived from Drop-Size Spectra," Final Report (Tech. Rep. ECOM-02071-F), Illinois State Water Survey at the University of Illinois, Urbana, May 1969, 112 pp.

Probert-Jones, J. R., "The Radar Equation in Meteorology," Quarterly Journal of the Royal Meteorological Society, Vol. 88, No. 378, 1962, pp. 485-495.

Rasmusson, Eugene M., "Mass, Momentum, and Energy Budget Equations for BOMAP Computations," NOAA Technical Memorandum ERL BOMAP-3, BOMAP Office, National Oceanic and Atmospheric Administration, U.S. Department of Commerce, Rockville, Md., January 1971, 32 pp.

Rasmusson, Eugene M., "Sub-Gridscale Fluxes of Momentum, Heat, and Water Vapor Derived From BOMEX Budget Analyses," NOAA Technical Report, 1975 (In preparation).

Sabatini, Romeo R., (ed.), The Nimbus III User's Guide, Goddard Space Flight Center, National Aeronautics and Space Administration, Greenbelt, Md., 237 pp.

Saunders, Peter M., "Some Characteristics of Tropical Marine Showers," Journal of the Atmospheric Sciences, Vol. 22, No. 2, 1965, pp. 167-175.

Scherer, Wolfgang D., and Michael D. Hudlow, BOMEX Period III Radar-Satellite Atlas, 1975, 47 pp.

Wilson, James W., "Integration of Radar and Raingage Data for Improved Rainfall Measurement," Journal of Applied Meteorology, Vol. 9, No. 3 1970, pp. 489-497.

Woodley, William L., John Norwood, and Briseida Sancho, "Some Precipitation Aspects of Florida Showers and Thunderstorms," Weatherwise, Vol. 24, No. 3, June 1971, pp. 106-114.

Woodley, W. L., B. Sancho, and A. H. Miller, "Rainfall Estimation From Satellite Cloud Photographs," NOAA Technical Memorandum ERL OD-11, Environmental Research Laboratories of NOAA, Boulder, Colo., February 1972, 43 pp.